

# **Tool to Estimate Land Surface Emissivity at Microwaves and Millimeter waves**

**TELSEM<sup>2</sup>**

March 2016

Catherine Prigent and Filipe Aires

A report for EUMETSAT

EUMETSAT Project EUM/CO/14/4600001473/CJA  
« Study on surface emissivity at microwave and sub-millimeter frequencies ».

## Table of Contents

<b>1. Introduction .....</b>	<b>3</b>
1.1. Scope of the document .....	3
1.2. Software version identification.....	3
1.3. References.....	3
<b>2. The microwave to millimeter-wave emissivity parameterization .....</b>	<b>3</b>
2.1. Goal of the Emissivity parameterization.....	3
2.2. SSM/I MW emissivity dataset description.....	4
2.3. Description of the parameterization scheme.....	5
2.4. Different configurations for the parameterization .....	5
2.5. Examples of parameterized emissivities .....	6
2.6. Parameterization of the uncertainties .....	7
2.7. List of inputs/outputs for the parameterization.....	8
2.8. Implementation of the parameterization.....	9
2.8.1. Installation.....	9
2.8.2. Structure of the library .....	9
2.8.3. Execution step.....	11
<b>Annexe 1: References.....</b>	<b>12</b>
<b>Annexe 2: Example for uncertainty calculations .....</b>	<b>13</b>
<b>Annexe 3: Paper Prigent et al., 2008. .....</b>	<b>16</b>
<b>Annexe 4: Paper Aires et al., 2011.....</b>	<b>25</b>

# 1. Introduction

## 1.1. Scope of the document

This document describes a land and sea-ice surface emissivity parameterization for the microwaves to the sub-millimeter waves attached to RTTOV, along with the emissivity climatology to which it is anchored. It provides the necessary technical information for the user who wishes to use this tool.

TELSEM is an official package of two community codes RTTOV and CRTM. TELSEM<sup>2</sup>

A similar tool, TESSEM<sup>2</sup> (Tool to Estimate Sea Surface Emissivity in the Microwaves and Millimeter waves), is also available for oceanic surfaces.

## 1.2. Software version identification

The current version of the software is 2.0.

## 1.3. References

- Aires, F., C. Prigent, F. Bernardo, C. Jimenez, R. Sounders, and P. Brunel, *A Tool to Estimate Land Surface Emissivities in the Microwaves (TELSEM) for use in numerical weather prediction schemes*. Q. J. Royal Meteor. Soc., 137: 690-699, DOI: 10.1002/qj.803, 2011.
- Prigent, C., E. Jaumouille, F. Chevallier, and F. Aires, *A parameterization of the microwave land surface emissivity between 19 and 100 GHz, anchored to satellite-derived estimates*, IEEE Transaction on Geoscience and Remote Sensing, 46, 344-352, 2008.
- A scientific paper on TELSEM<sup>2</sup> is in preparation.

# 2. Land microwave to millimeter-wave emissivity parameterization

## 2.1. Goal of the Emissivity parameterization

The goal of the emissivity parameterization is to provide a first-guess of the microwave to millimeter-wave emissivity for simulation purposes of satellite observations, for its use in inversion algorithms, and as a tool for variational assimilation.

The parameterization was originally designed for frequencies between 19 and 85 GHz (TELSEM). Preliminary tests showed that for most surface types it was valuable down to 10 GHz and up to 190 GHz (see e.g. Bernardo, Aires, and Prigent, *Atmospheric water vapour retrieval from microwave instruments - Part II: Evaluation for the Megha-Tropiques mission*, QJRMS, DOI: 10.1002/qj.1946, 2012), as tested with AMSR-E and AMSU-B frequencies. The version 2.0 parameterization is now extended to sea-ice, and the frequency extrapolation to high frequencies has been explored and refined, using

AMSU-B and SSMI/S satellite-derived emissivities. A paper is in preparation to describe this new parameterization.

## 2.2. SSM/I MW emissivity dataset description

The parameterization is anchored to a monthly-mean climatology of emissivities calculated from SSM/I observations at SSM/I frequencies (19, 22, 37 and 85 GHz for vertical and horizontal polarizations, except for 22 GHz which is vertical only), with a spatial resolution of  $0.25^\circ \times 0.25^\circ$  at the equator (equal area grid). This climatology has been computed by averaging 8 years of SSM/I monthly-mean emissivities (from 1993 to 2000, see references in annexe 1). This climatology is distributed with the emissivity parameterization. The ASCII files content is described in the following table:

Cell number	Number of the cell in the $0.25^\circ \times 0.25^\circ$ equal-area grid
Emis19V	Emissivity at 19 GHz for vertical polarization
Emis19H	Emissivity at 19 GHz for horizontal polarization
Emis22V	Emissivity at 22 GHz for vertical polarization
Emis37V	Emissivity at 37 GHz for vertical polarization
Emis37H	Emissivity at 37 GHz for horizontal polarization
Emis85V	Emissivity at 85 GHz for vertical polarization
Emis85H	Emissivity at 85 GHz for horizontal polarization
VAR Emis19V	Variance <sup>1</sup> of the emissivity at 19 GHz V used as uncertainty
VAR Emis19H	Variance of the emissivity at 19 GHz H used as uncertainty
VAR Emis22V	Variance of the emissivity at 22 GHz V used as uncertainty
VAR Emis37V	Variance of the emissivity at 37 GHz V used as uncertainty
VAR Emis37H	Variance of the emissivity at 37 GHz H used as uncertainty
VAR Emis85V	Variance of the emissivity at 85 GHz V used as uncertainty
STD Emis85H	Variance of the emissivity at 85 GHz H used as uncertainty
Surface class1	Surface class1 is used for the angular and polarization parameterization. It is equal to the variable class in the previous version of the parameterization (TELSEM), and for uncertainty assessment.  From 1 to 5 snow and ice-free regions from highly vegetated to desert, from 6 to 9 various snow and ice types (including sea-ice), and class 10 for pixels containing standing water.

---

<sup>1</sup> Please note that the original climatology files provide the variance of the emissivity uncertainties but that the interpolator converts right away, during the reading of this to the emissivity uncertainty standard-deviation.

Surface class2      Surface class2 is used for the frequency parameterization. From 1 to 5 snow and ice-free regions from highly vegetated to desert (equal to class1). Class 10 for pixel with standing water. Classes 11 to 16 for sea-ice. Classes 17 to 22 for continental snow and ice. Classes 6 to 9 in TELSEM corresponded to snow and ice. These surface types have been reclassified into 6 classes for a better discrimination of the surfaces and are numbered from 17 to 22. To avoid confusion, numbers from 6 to 9 are not used in class2 of TELSEM<sup>2</sup>.

For each surface type, Table 1 gives the surface class as described in the EUMETSAT Final report (2016), the TELSEM<sup>2</sup> class1 index, the TELSEM<sup>2</sup> class2 index, and the major characteristics of each surface. TELSEM class indicates the class numbering in the old version of TELSEM.

Surface type	Class nb for each type	Class1 in TELSEM <sup>2</sup>	Class2 in TELSEM <sup>2</sup>	Broad characteristics
Sea-ice	1	10	11	Sea-ice margining
	2	10	12	New sea-ice
	3	10	13	New sea-ice
	4	9	14	Multi-year sea-ice
	5	8	15	Multi-year sea-ice
	6	7	16	Multi-year sea-ice
Snow and continental ice	1	TELSEM class	17	Snow (small grain)
	2	TELSEM class	18	Snow (medium grain)
	3	TELSEM class	19	Snow (large grain)
	4	TELSEM class	20	Continental ice
	5	TELSEM class	21	Continental ice
	6	TELSEM class	22	Continental Ice
Continents (snow and ice-free)	1	1	1	Tropical forest
	2	2	2	Dense vegetation
	3	3	3	Bushes
	4	4	4	Grassland
	5	5	5	Deserts
	6	10	10	Water surfaces

A file (correlations) is also distributed to provide the 7×7 correlation matrices of the SSM/I emissivity uncertainties, for each of the surface class1.

### 2.3. Description of the parameterization scheme

See annexe 3.

### 2.4. Different configurations for the parameterization

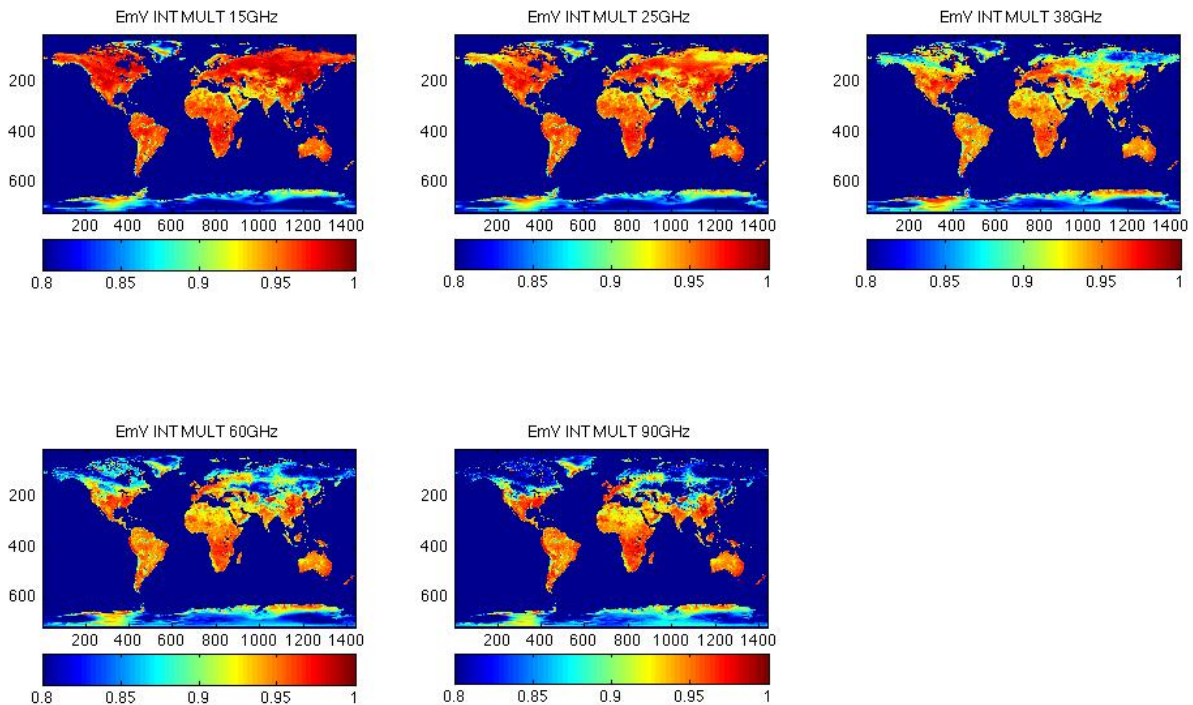
Four configurations have been considered for the emissivity parameterization to facilitate and optimize its use, depending on the various applications that can utilize the parameterization. These 4 configurations are:

- **IND\_SING**: when the location and frequency are specified, the parameterization uses an INDividual atlas-pixel (i.e. nearest location in the equal-area grid), and estimates a SINGLE frequency emissivity.  
→ *emis\_interp\_ind\_sing(lat, lon, theta, freq, atlas, ev, eh, stdv, stdh, verb)*

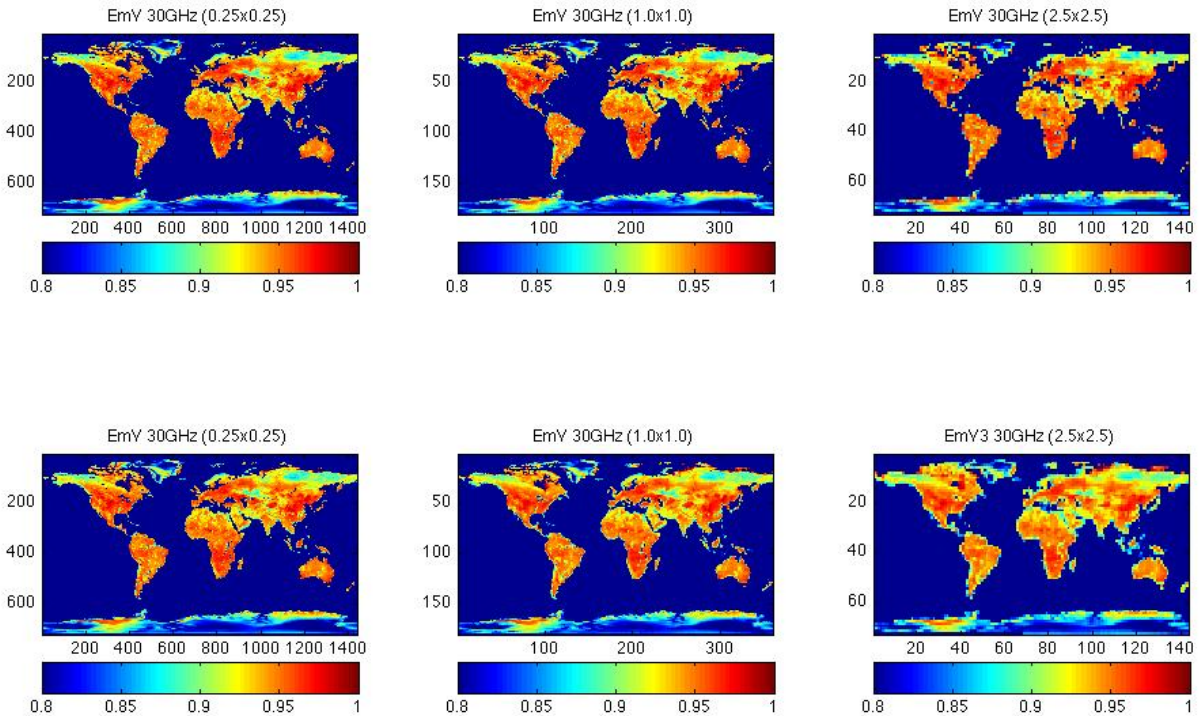
- **INT\_SING**: In this configuration again, only one frequency is considered but the parameterization INTEGRATES multiple atlas pixels taking into account the resolution that is specified. If the spatial resolution is higher than the  $0.25^\circ \times 0.25^\circ$  spatial resolution of the initial dataset, the pixels that fall into the new spatial grids are averaged. If the spatial resolution is lower than the  $0.25^\circ \times 0.25^\circ$  initial spatial resolution, the nearest pixel is considered.  
→ *emis\_interp\_int\_sing(lat, lon, resol, theta, freq, atlas, ev, eh, stdv, stdh, verb)*
- **IND\_MULT**: The nearest atlas-pixel is used here to parameterize at MULTiple frequencies.  
→ *emis\_interp\_ind\_mult(lat, lon, theta, freq, n\_chan, atlas, ev, eh, std, verb)*
- **INT\_MULT**: The INTEGRATION of the atlas-pixels is used to parameterize MULTiple frequencies.  
→ *emis\_interp\_int\_sing(lat, lon, resol, theta, freq, atlas, ev, eh, std, verb)*

## 2.5. Examples of parameterized emissivities

In the following figures, the INT\_MULT parameterization configuration is used to estimate the emissivities at 15, 25, 38, 60 and 90 GHz at vertical polarization.



The next figures give examples of emissivity estimates for 30 GHz at vertical polarization for horizontal resolutions, from left to right, of  $0.25^\circ \times 0.25^\circ$ ,  $1.0^\circ \times 1.0^\circ$  and  $2.5^\circ \times 2.5^\circ$ ; top 3 maps are for the IND configuration (nearest atlas-pixels), and bottom 3 maps are for the INT configuration (i.e., integration of the atlas pixels).



## 2.6. Parameterization of the uncertainties

Let  $\text{EM}_{\text{SSMI}}(6)$  be the 6-channels SSM/I emissivities from the atlas (19V, 37V, 85V, 19H, 37H and 85H). The goal of the emissivity parameterization is to estimate a new emissivities  $\text{EM}_{\text{NEW}}(f)$  at frequency  $f$ . The first half of  $\text{EM}_{\text{NEW}}$  is for vertical and the second half for horizontal polarizations. How is the new uncertainty covariance matrices computed?

In order to estimate the emissivities at new frequencies (and scanning angle and polarization), the parameterization uses a  $(f \times 6)$  matrix, FIM, such that:

$$(\text{EmV}; \text{EmH}) = \text{FIM} \bullet \text{EM}_{\text{SSMI}}$$

From the SSMI atlas, we have the  $6 \times 6$  correlation matrix:

$$\text{COR}_{\text{SSMI}}(6,6)$$

for the uncertainties on the 6 SSMI channels and the associated vector of uncertainty standard deviation is defined by:

$$\text{STD}_{\text{SSMI}}(6)$$

The covariance matrix of the new emissivity uncertainties can be estimated using:

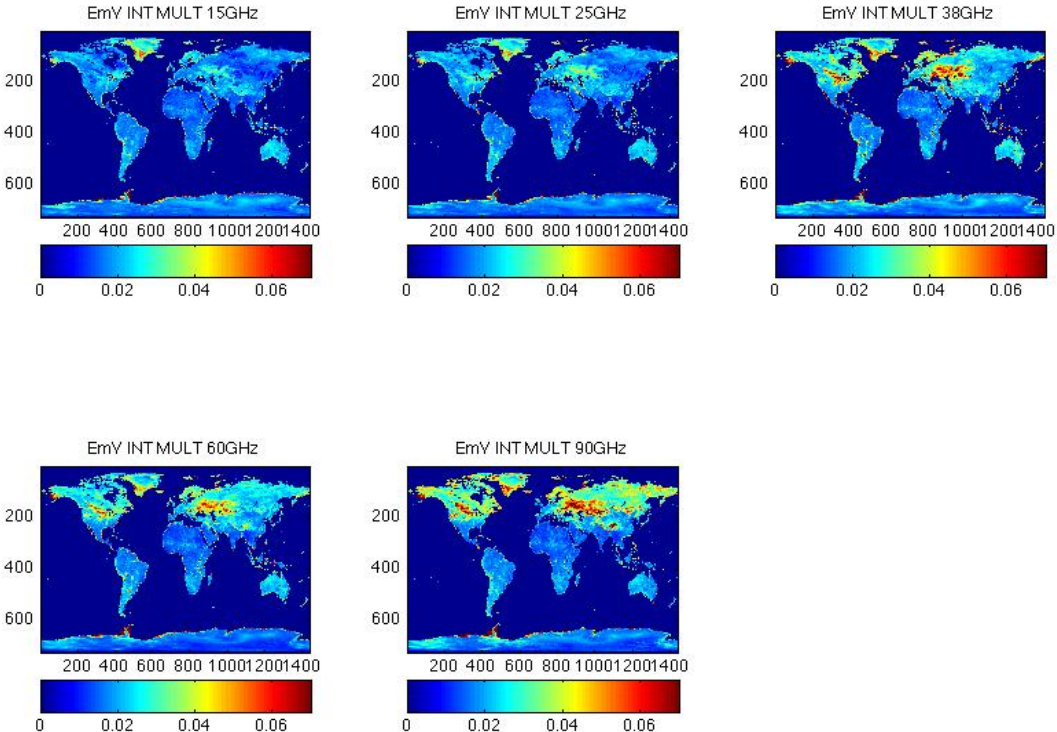
$$\text{COV}_{\text{SSMI}} = \text{STD}'_{\text{SSMI}} \bullet \text{COR}_{\text{SSMI}} \bullet \text{STD}_{\text{SSMI}}$$

The covariance matrix of the new emissivity uncertainties can be estimated using:

$$\text{COV}_{\text{NEW}} = \text{FIM}' \bullet \text{COV}_{\text{SSMI}} \bullet \text{FIM} = \text{FIM}' \bullet \text{STD}'_{\text{SSMI}} \bullet \text{COR}_{\text{SSMI}} \bullet \text{STD}_{\text{SSMI}} \bullet \text{FIM}$$

In order to better explain this process, an example of such computations is given in Annexe 2.

The following figure gives the uncertainty estimates for the parameterization at 15, 25, 38, 60 and 90 GHz.



## 2.7. List of inputs/outputs for the parameterization

Real Latitude: [-90; 90]

Real Longitude: [0; 360]

Real Theta [0; 90°]      ! Incidence angle

Real freq[19; 85]      ! Freq to parameterize. It is possible to use lower or higher freq.

! -----For individual freq parameterization

Real ev, eh, stdv, stdh      ! Interpolated emissivities with uncertainties

!----- For multiple freq parameterization

Real resol      ! Horizontal resolution for the user

Integer n\_chan=5      !Number of channel to interpolate

Real ev(5), eh(5), std(2\*5,2\*5)      !parameterized emissivities with uncertainties

Real freq2(5)      !Frequencies for the parameterization

## 2.8. Implementation of the parameterization

### 2.8.1. Installation

The atlas (12 monthly-mean emissivity files and the correlations file) can be copied in any location. The library needs to be compiled with

```
g95 -c mod_mwatlas_M2.f90
```

The compilation of the Fortran code, *test*, that will ask for the library needs to be compiled with:

```
g95 -o test mod_mwatlas_M2.o test.o
```

### 2.8.2. Structure of the library

At the heart of the library is the structure `Atlas_emis_mw` that represents the microwave emissivity atlas. This structure is composed by:

TYPE <code>atlas_emis_mw</code>		
Type	Array name	Contents
INTEGER	Ndat	Number of lines in the atlas
INTEGER	Nchan	Number of channels in the atlas
CHARACTER(len=22)	Name	Name of the atlas (including version number)
INTEGER	Month	Month of the atlas
REAL	Dlat	Resolution of the atlas (equal-area)
INTEGER, POINTER	ncells(:)	Number of cells per lat band
INTEGER, POINTER	Firstcell(:)	The first cell number of lat band
REAL	lat1, lat2, lon1, lon2	Limits of the spatial domain (flagged if global)
REAL, POINTER	emis(ndat,nchan)	Emissivities
REAL, POINTER	correl(10,nchan,nchan)	Correlations or uncertainties for each surface class1
REAL, POINTER	emis_err(ndat,nchan)	Emissivity uncertainties (std)

INTEGER, POINTER	Class1(ndat)	Surface class1 (1-10)
INTEGER, POINTER	Class2(ndat)	Surface class2 (1-22)
INTEGER, POINTER	Cellnum(ndat)	Cell number of each pixel in the atlas
INTEGER	correspondance(660066)	"Correspondance" vector indicating that for the $i^{th}$ element, the $j$ so that $EMIS(j,...)$ is the emissivity of cell number $i$ .

The codes are in a library « mod\_mwatlas\_M2.f90 ».

- SUBROUTINE **rttov\_readmw\_atlas**(dir,month,atlas,error\_status,lat1,lat2,lon1,lon2)  
 These routines read the emissivity atlas, including the emissivities, the associated standard deviations for uncertainties and the correlation matrices for uncertainties for each surface type (see files in section 2.2). The user can specify a zone (lat1, lat2, lon1 and lon2) to download only a limited amount of the atlas.
- SUBROUTINE **equare**(DLAT,NCELLS,FIRSTCELL)  
 This routine computes the number of cells and the first cell number for each latitude band. This procedure is for equal-area grids such as for the SSM/I microwave atlas provided in this package. As an example, for a  $0.25^\circ \times 0.25^\circ$  equal-area grid, there are 720 latitude bands, NCELLS(720) gives the numbers of pixels for each band, and FIRSTCELL(720) gives the cell number of the first pixel in a latitude band.
- FUNCTION **calc\_cellnum**(lat,lon,atlas)  
 This routine computes the cell number from the lat and lon. This procedure uses the NCELLS included in the atlas, and computed once and for all by routine EQUARE during the atlas reading (rttov\_readmw\_atlas).
- SUBROUTINE **calc\_cellnum\_mult**(lat,lon,resol,atlas,cell\_num\_mult,nb\_cell)  
 This routine is similar to function CALC\_CELLNUM but it computes the list of cell numbers from the latitude, longitude and resolution (desired spatial resolution of the outputs). It gives for each cell of the new grid the cell numbers of the pixels in the initial grid to be averaged. This routine uses the NCELLS and FIRSTCELLS included in the atlas.
- SUBROUTINE **interp\_freq2**(emiss19,emiss37,emiss85,f,emiss,an,bn,cn)  
 This routine computes the linear parameterization of emissivity given the frequency and the atlas values for that cell number.
- SUBROUTINE **emis\_interp**(lat,lon,theta,freq,class1,class2,ev,eh,emiss\_interp\_v,emiss\_interp\_h)  
 This routine performs the parameterization of emissivity in angle and frequency.
- SUBROUTINE **emis\_interp\_ind\_sing**(lat,lon,theta,freq,atlas,ev,eh,stdv,stdh,verb)  
 Parameterizes emissivity for:  
   IND: individual atlas-pixel  
   SING: singular channel
- SUBROUTINE **emis\_interp\_int\_sing**(lat,lon,resol,theta,freq,atlas,ev,eh,stdv,stdh,verb)  
 Parameterizes emissivity for:  
   INT: integrate atlas-pixel  
   SING: singular channel

- SUBROUTINE **emis\_interp\_ind\_mult**(lat,lon,theta,freq,n\_chan,atlas,ev,eh,std,verb)  
Parameterizes emissivity for:  
    IND: individual cell number atlas-pixel  
    MULT: multiple channel
- SUBROUTINE **emis\_interp\_int\_mult**(lat,lon,resol,theta,freq,atlas,ev,eh,std,verb)  
Parameterizes emissivity for:  
    INT: integrate atlas-pixel  
    MULT: multiple channel

### 2.8.3. Execution step

Please, see example in file test.f90

## Annexe 1: References

- Prigent, C., P. Liang, Y. Tian, F. Aires, J.-L. Moncet, and S.-A. Boukabara, Evaluation of modeled microwave land surface emissivity with satellite-derived estimates, *J. Geophys. Res. Atmos.*, 120, 2706-2718, doi: 10.1002/2014JD021817, 2015.
- Aires, F., C. Prigent, F. Bernardo, C. Jimenez, R. Saunders, and P. Brunel, A Tool to Estimate Land-Surface Emissivities at Microwave frequencies (TELSEM) for use in numerical weather prediction, *Q. J. R. Meteorol. Soc.*, 137:690-699, 2011.
- Prigent, C., E. Jaumouille, F. Chevallier, and F. Aires, A parameterization of the microwave land surface emissivity between 19 and 100 GHz, anchored to satellite-derived estimates, *IEEE TGRS*, 46, 344-352, 2008.
- Prigent, C., F. Aires, and W. B. Rossow, Land surface microwave emissivities over the globe for a decade, *Bul. Amer. Meteorol. Soc.*, doi:10.1175/BAMS-87-11-1573, 1573-1584, 2006.
- Prigent, C., Microwave emissivity in arid reagions, what can we learn from satellite observations?, Chap. 4.5 in "Thermal Microwave Radiation - Applications for Remote Sensing", Matzler, C., P.W. Rosenkranz, A. Battaglia, and J.P. Wigneron (eds.), IEE Electromagnetic Waves Series 52, London, UK, 2006.
- Prigent, C., Passive microwave emissivity in vegetated reagions as directly calculated from satellite observations, Chap. 4.6, in "Thermal Microwave Radiation - Applications for Remote Sensing", Matzler, C., P.W. Rosenkranz, A. Battaglia, and J.P. Wigneron (eds.), IEE Electromagnetic Waves Series 52, London, UK, 2006.
- Prigent, C., J. Munier, B. Thomas, and G. Ruffié, Microwave signatures over carbonate sedimentary platforms in arid areas: Potential geological applications of passive microwave observations?, *Geophys. Res. Lett.*, 32, L23405, doi:10.1029/2005GL024691, 2005.
- Karbou, F., and C. Prigent, Calculation of microwave land surface emissivity from satellite observations: validity of the specular approximation over snow-free surfaces? *IEEE Geoscience Remote Sensing Letters*, 2, 311-314, 2005.
- Prigent, C., F. Chevallier, F. Karbou, P. Bauer and G. Kelly, AMSU-A land surface emissivity estimation for numerical weather prediction assimilation schemes, *Journal of Applied Meteorology*, 44, 416-426, 2005.
- Karbou, F., C. Prigent, L. Eymard, and J. Pardo, Microwave land emissivity calculations using AMSU measurements, *IEEE TGRSE*, 43, 5, 948- 959, 2005.
- Aires, F., C. Prigent, W. B. Rossow, M. Rothstein, A new neural network approach including first-guess for retrieval of atmospheric water vapor, cloud liquid water path,surface temperature and emissivities over land from satellite microwave observations, *Journal of Geophysical Research*, 106, 14 887-14 907, 2001.
- Prigent, C., J.P. Wigneron, W. B. Rossow, J. R. Pardo-Carrion, Frequency and angular variations of land surface microwave emissivities: Can we estimate SSM/T and AMSU emissivities from SSM/I emissivities?, *IEEE Transactions on Geoscience and Remote Sensing*, 38, 2373-2386, 2000.
- Prigent, C., W. B. Rossow, E.Matthews, Global maps of microwave land surface emissivities: Potential for land surface characterization, *Radio Science*, 33, 745-751, 1998.
- Prigent C., W. B. Rossow, E. Matthews, Microwave land surface emissivities estimated from SSM/I observations, *Journal of Geophysical Research*, 102, 21867-21890, 1997.

## Annexe 2: Example for uncertainty calculations

How are the uncertainty covariance matrices computed? The emissivities for new frequencies are first computed:

Frequency	15 GHz	25 GHz	38 GHz	60 GHz	90 GHz
Emis V	0.9603142	0.9595809	0.9588379	0.9618543	0.9659674
Emis H	0.9590667	0.9586814	0.9583531	0.9613068	0.9653345

From the SSMI atlas, we have the 6x6 covariance matrix Cov<sub>SSMI</sub> and the correlation matrix Cor<sub>SSMI</sub> for the uncertainties on the 6 SSM/I channels (19, 37 and 85 GHz for both V and H polarizations).

Em19V	0.0004	0.0004	0.0004	0.0004	0.0004	0.0004
Em37V		0.0005	0.0004	0.0005	0.0005	0.0005
Em87V			0.0004	0.0004	0.0005	0.0005
Em19H				0.0005	0.0005	0.0005
Em37H					0.0010	0.0009
Em87H						0.0010

And the associated correlation matrix:

Em19V	<b>1.00</b>	0.96	0.96	0.94	0.72	0.73
Em37V		<b>1.00</b>	0.95	0.95	0.71	0.72
Em87V			<b>1.00</b>	0.96	0.79	0.79
Em19H				<b>1.00</b>	0.76	0.78
Em37H					<b>1.00</b>	0.93
Em87H						<b>1.00</b>

The “interpolation” matrix FIM is given by:

**1.0000** 0.0000 0.0000 0.0000 0.0000 0.0000

<b>0.6799</b>	<b>0.3201</b>	0.0000	0.0000	0.0000	0.0000
0.0000	<b>0.9794</b>	<b>0.0206</b>	0.0000	0.0000	0.0000
0.0000	<b>0.5258</b>	<b>0.4742</b>	0.0000	0.0000	0.0000
0.0000	0.0000	<b>1.0000</b>	0.0000	0.0000	0.0000
0.0000	0.0000	0.0000	<b>1.0000</b>	0.0000	0.0000
0.0000	0.0000	0.0000	<b>0.6799</b>	<b>0.3201</b>	0.0000
0.0000	0.0000	0.0000	0.0000	<b>0.9794</b>	<b>0.0206</b>
0.0000	0.0000	0.0000	0.0000	<b>0.5258</b>	<b>0.4742</b>
0.0000	0.0000	0.0000	0.0000	<b>1.0000</b>	

And the new covariance matrix is estimated by:

Cov=10<sup>-4</sup>.

Em15V	4	4	4	4	4	4	4	4	4	4
Em25V		4	4	4	4	4	4	5	5	5
Em38V			5	5	4	5	5	5	5	5
Em60V				4	4	4	4	5	5	5
Em90V					4	4	4	5	5	5
Em15H						5	5	5	5	5
Em25H							5	7	7	7
Em38H								10	10	9
Em60H									10	10
Em90H										10

That corresponds to a correlation matrix:

Em15V	<b>1.00</b>	0.995	0.960	0.972	0.960	0.940	0.904	0.721	0.737	0.730
Em25V		<b>1.00</b>	0.983	0.987	0.965	0.952	0.913	0.724	0.741	0.733
Em38V			<b>1.00</b>	0.991	0.951	0.951	0.908	0.713	0.729	0.721
Em60V				<b>1.00</b>	0.984	0.966	0.936	0.755	0.771	0.760
Em90V					<b>1.00</b>	0.960	0.947	0.791	0.804	0.790

Em15H	<b>1.00</b>	0.959	0.761	0.783	0.780
Em25H		<b>1.00</b>	0.913	0.919	0.780
Em38H			<b>1.00</b>	0.919	0.932
Em60H				<b>1.00</b>	0.980
Em90H					<b>1.00</b>

## Annexe 3: Paper Prigent et al., 2008.

344

IEEE TRANSACTIONS ON GEOSCIENCE AND REMOTE SENSING, VOL. 46, NO. 2, FEBRUARY 2008

# A Parameterization of the Microwave Land Surface Emissivity Between 19 and 100 GHz, Anchored to Satellite-Derived Estimates

Catherine Prigent, Elodie Jaumouillé, Frédéric Chevallier, and Filipe Aires

**Abstract**—Land surface emissivities have been calculated for Tropical Rainfall Measuring Mission (TRMM) Microwave Instrument (TMI), Special Sensor Microwave/Imager (SSM/I), and Advanced Microwave Sounder Unit-A conditions, for two months (July 2002 and January 2003) over the globe at the European Centre for Medium-Range Weather Forecasts, directly from satellite observations. From this data set, a parameterization of the microwave emissivities that account for frequency, incidence angle, and polarization dependences is proposed. It is anchored to climatological monthly mean maps of the emissivities at 19, 37, and 85 GHz, which are calculated from SSM/I. For each location and time of the year, it provides realistic first-guess estimates of the microwave emissivities from 19 to 100 GHz, for all scanning conditions. The results are compared to radiative transfer model estimates. The new estimates provide rms errors that are usually within 0.02, with the noticeable exception of snow-covered regions where the high spatial and temporal variabilities of the emissivity signatures are difficult to capture.

**Index Terms**—Emissivity, land surface, microwave.

## I. INTRODUCTION

FOR A large range of applications, there is a need for land surface microwave emissivity estimates, for all observation angles and polarizations, for the whole globe. Surface-sensitive microwave channels from satellite-borne instruments contain some key information about surface temperature, lower troposphere temperature, cloud liquid water, and precipitating water. Accurate microwave land surface emissivities are essential to properly extract such information in 1-D retrievals or within complex 4-D data assimilation systems in Numerical Weather Prediction (NWP) centers. The interaction between microwave radiation and the land surface is complex, being dependent on a large number of highly variable surface characteristics, such as soil humidity and roughness, vegetation properties, or snow cover. An extensive body of research has been directed toward a better understanding of the mechanisms

responsible for the microwave emission of land surfaces, from field experiments (using ground-based [1] or airborne sensors [2]), from radiative transfer modeling [3], [4], and from emissivity estimates derived from satellite observations [5]–[7].

Field experiments, which are under controlled conditions, provide high temporal and spatial resolution of the surface emissivity and make it possible to analyze the effect of detailed surface processes on the surface emissivity (e.g., freeze-thaw cycle, leaf orientation, or rain effect). However, they are performed for a limited number of surface types, observed under specific conditions (frequency and incidence angle), and have a difficulty in encompassing the large spatial and temporal variability of the surfaces measured from satellites at a global scale.

Land surface emissivity models have been developed for the globe for various surface conditions encountered over the continents [4], [8], using different radiative transfer solutions depending on the surface characteristics. Model inputs are provided by a land surface model, such as the one in the Global Data Assimilation System of the National Center for Environmental Prediction (NCEP) [4]. For specific surfaces and regional applications, coupling of land surface outputs with a radiative model can be efficient [9]. However, even when assuming that a perfect land surface emissivity model exists, the inputs it will require on a global basis (e.g., soil composition, texture, humidity, or roughness, vegetation and snow characteristics) would not be easily available with the spatial resolution compatible with the satellite and with the required accuracy.

Global land surface emissivity maps have been produced directly from satellite observations. For instance, emissivity atlases are calculated from Special Sensor Microwave/Imager (SSM/I) measurements [5], [7], by removing the contribution of the atmosphere, clouds, rain, and the surface temperature, using ancillary data. The emissivities are estimated for SSM/I observation conditions, i.e., between 19 and 85 GHz at 53° incidence angle, and for both vertical and horizontal polarizations. Advanced Microwave Sounder Unit (AMSU) emissivities have also been calculated [6], [10]. However, these satellite estimates are limited to the observation conditions of the given satellite (frequency, incidence angle, and polarization). For a given period of time, AMSU only provides a limited number of overpasses of the same location with the same incidence angle and does not give access to the vertical and horizontal polarization information separately. In addition, direct calculation of the emissivities from satellite observations requires a large amount of ancillary information that is not always easily accessible.

Manuscript received January 18, 2007; revised July 19, 2007.

C. Prigent and E. Jaumouillé are with the Laboratoire d'Etudes du Rayonnement et de la Matière en Astrophysique, Paris Observatory, Centre National de la Recherche Scientifique, 75014 Paris, France.

F. Chevallier is with the Laboratoire des Sciences du Climat et de l'Environnement, Commissariat à l'Energie Atomique, Centre National de la Recherche Scientifique, Université de Versailles Saint-Quentin-en-Yvelines, Institut Pierre-Simon Laplace, F-91191 Gif-Sur-Yvette Cedex, France.

F. Aires is with the Centre National de la Recherche Scientifique, Institut Pierre-Simon Laplace, Laboratoire de Météorologie Dynamique, F-75252 Paris Cedex 05, France.

Digital Object Identifier 10.1109/TGRS.2007.908881

Good cloud filtering and a reliable surface skin temperature are particularly needed.

In order to provide the community with land surface emissivity estimates for the globe for all observing conditions (incidence angles and polarizations) between 19 and 100 GHz, we propose to derive a parameterization of the frequency, angular, and polarization dependences of the emissivity, anchored on a reliable satellite-derived emissivity database. First, satellite-derived estimates of the land surface emissivities are calculated from Tropical Rainfall Measuring Mission (TRMM) Microwave Instrument (TMI), SSM/I, and AMSU-A observations, for two months (July 2002 and January 2003) for the globe to analyze the frequency, angular, and polarization dependences for the different land surface types. A parameterization of the emissivity frequency, angular, and polarization dependences is deduced for each surface type. This parameterization along with the previously calculated SSM/I emissivity climatology at 19, 37, and 85 GHz for both polarizations at 53° provides an emissivity estimate for all locations on Earth for each month of the year, for all the incidence angles and polarizations between 19 and 100 GHz. The results are compared with model outputs.

## II. EMISSIVITY DATA SETS

For a comprehensive analysis of the emissivity variations with surface type, frequency, angle, and polarization, this study examines and compares several sources of land surface microwave emissivity estimates, including satellite-derived values and model results.

### A. Satellite-Derived Emissivity Data Sets

*1) SSM/I, TMI, and AMSU-A Emissivity Database:* In order to examine the frequency, angular, and polarization dependences for the full range of possible land surface conditions, microwave emissivities have been calculated at the European Centre for Medium Range Weather Forecasts (ECMWF) for all continents for two contrasted months (July 2002 and January 2003) from the satellite measurements derived from the following three instruments that have different observing conditions: SSM/I, TMI, and AMSU-A.

The Special Sensor Microwave/Imager (SSM/I) onboard the Defense Meteorological Satellite Program (DMSP) polar orbiters observes the Earth twice daily at 19.35, 22.235, 37.0, and 85.5 GHz with both the vertical and horizontal polarizations, with the exception of the 22 GHz (vertical polarization only). The observing incidence angle is close to 53°, and the fields of view decrease with frequency, from 43 × 69 km to 13 × 15 km [11].

The TMI is similar to SSM/I, with the addition of a lower frequency channel, a tropical orbit, and a better spatial resolution. It measures the microwave radiation in the tropical region from ∼40° S to ∼40° N, at five frequencies, 10.65, 19.35, 21.30, 37.00, 85.50 GHz, for both the vertical and horizontal polarizations (except at the 21.30 GHz which is only observed in the vertical polarization). The incidence angle is ∼53°. The spatial resolution ranges from 36.8 × 63.2 km at 10.65 GHz to 4.6 × 7.2 km at 85.50 GHz.

The AMSU-A onboard the NOAA polar orbiters provides atmospheric temperature profiling capabilities [12]. The window channels are at 23.8, 31.4, and 89 GHz. It is a cross-track scanning instrument, with 30 scan positions at 3.3° intervals from  $-14.5 \times 3.3^\circ$  to  $+14.5 \times 3.3^\circ$  which translate into local zenith angles  $\theta_z$  up to 58.5°. The spatial resolution is 50 km at nadir. The polarization measured by AMSU-A rotates with the scan angle due to the rotating-reflector/fixed-feed type of antenna design and is a known mix of the vertical and horizontal polarizations (see [10] for more details).

The emissivity calculation method follows closely the scheme that was previously developed for SSM/I, which is described in detail in [5] and [7]. In this work, the selection of the clear pixels is based on the forecast model at ECMWF (not on the cloud flag from the International Satellite Cloud Climatology Project (ISCCP) [13] like in the previous work with SSM/I as this information is not available on real time to NWP centers). The observations that correspond to a nonzero fractional area cloud cover in the model are excluded. The atmospheric contribution is calculated from the ECMWF forecast model variables using the radiative transfer for the Tiros Operational Vertical Sounder (RTTOV) [14], [15].

An example of satellite-derived emissivity maps, which were calculated under clear-sky conditions and averaged over July 2002, is presented at 31.4 GHz from the AMSU-A observations for the incidence angles between 10° and 20° (Fig. 1). The holes in the maps correspond to the regions that are considered persistently cloudy during the month by the ECMWF forecast model.

*2) Reference SSM/I-Derived Emissivity Database Over a Decade:* The microwave land surface emissivities have been calculated over the globe for approximately ten years between 19 and 85 GHz at a 53° incidence angle for both vertical and horizontal polarizations using SSM/I observations. Ancillary data (ISCCP products [13] and NCEP reanalyses [16]) help remove the contribution from the atmosphere, clouds, and rain from the measured satellite signal and separate surface temperature from emissivity variations. This data set has been extensively evaluated (e.g., [7]), and in this study, it serves as a reference from which a monthly mean emissivity climatology is calculated and an emissivity-based surface-type classification is derived. This reference database is accessible at <http://geo.obspm.fr/>.

### B. Model-Derived Emissivity Database

For comparison purposes, the emissivities have also been calculated at ECMWF, using the radiative transfer model from Weng *et al.* [4] with the forecast-model-relevant surface variables (soil temperature and humidity, vegetation fraction, and snow depth) as inputs. This model uses different solutions depending on the surface type.

## III. ANALYSIS OF THE EMISSIVITY FREQUENCY AND ANGULAR DEPENDENCES

In order to facilitate the analysis of the frequency and angular dependences of the SSM/I, TMI, and AMSU emissivities, the data set is sorted per surface types. Instead of using an external

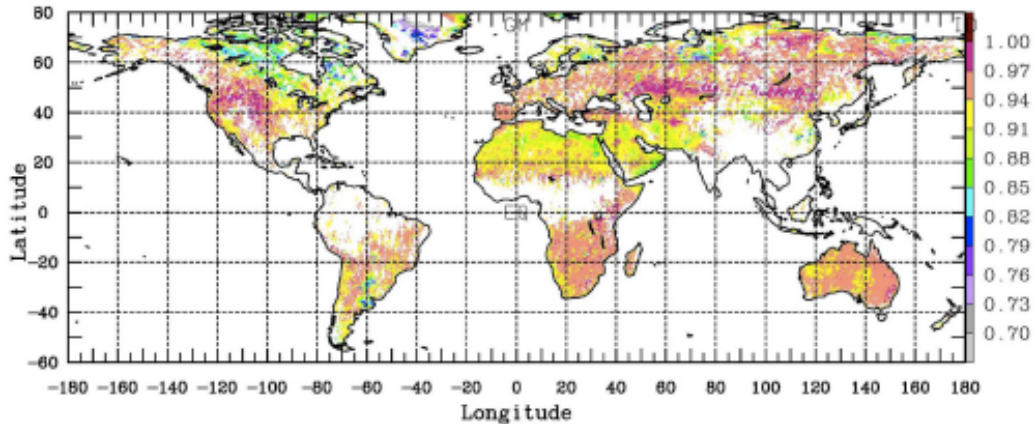


Fig. 1. Satellite-derived emissivity from AMSU-A at 31.4 GHz for July 2002 for the incidence angles between 10° and 20°.

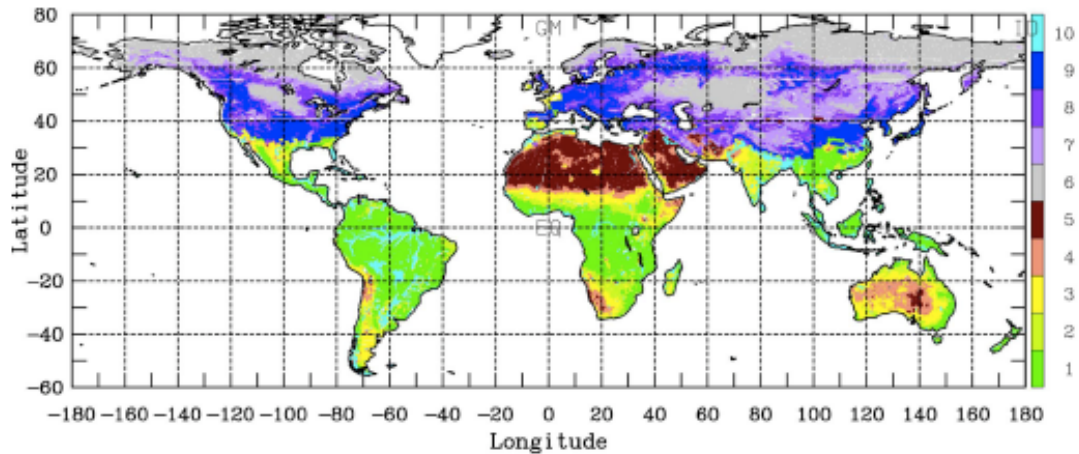


Fig. 2. Result of the classification of SSM/I derived emissivities for January. Classes from 1 to 5 represent continental snow-free regions. Classes 6 to 9 correspond to snow-covered land, and pixels with standing water are grouped in class 10.

and independent classification of vegetation, we develop a classification of the SSM/I emissivity, based on the reference SSM/I emissivity data set: this insures that each class represents a different behavior in terms of microwave emissivities and that the set of classes describes the full variability of these emissivities. The frequency and angular dependences of the satellite-derived emissivities are then analyzed for each surface type and compared to the model ones.

#### A. Classification of the Emissivity Data Set

The monthly mean emissivity climatology is calculated from the decadal (1992–2001) SSM/I emissivity database. An unsupervised clustering technique is applied to this emissivity climatology for the seven SSM/I channels. The chosen classification scheme (topological method from [17]) imposes a neighborhood requirement on nearby classes so that results are

easier to interpret (for more details on the classification method, see [18]). The clustering method is applied twice as follows: once for the snow-free pixels, then for the snow-covered pixel (the snow and ice information is extracted from the National Snow and Ice Data Center; ice pixels are not considered). Five classes are isolated for the snow-free regions, corresponding to vegetation densities, from dense vegetation (class 1) to desert surfaces (class 5), and four snow classes are also determined. Pixels with more than 10% standing water are not considered in the clustering scheme and are grouped in class 10: it includes areas of rivers or lakes, as well as regions associated with seasonal wetlands as defined by [19]. Fig. 2 shows the result of the classification for the month of January applied to the reference data set. The snow-free classes (from 1 to 5) show consistent spatial structures related to vegetation density. Note that given the small number of classes considered here and the limited sensitivity of the passive microwave observations

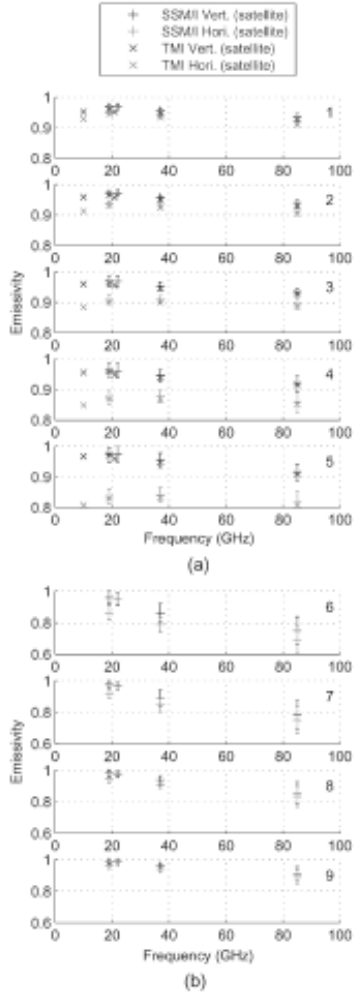


Fig. 3. Mean emissivity frequency dependence as observed from satellite-derived emissivities from the SSM/I and TMI at a 53° incidence angle, for both the vertical and horizontal polarizations for January 2003 (a) for the snow-free surface types and (b) for the snow-covered surfaces. The standard deviation is added for the SSM/I estimates.

at these frequencies to discriminate between very dense forest and moderate vegetation, most vegetated regions are grouped in classes 1 and 2. The snow classes as well present realistic structures, with class 6 related to dry and thick snow related to the strong scattering at 85 GHz, and class 9 associated to wet snow (see [20] for more details on the snow classification). We tried classifications with a higher number of classes, but this did not change significantly the final results of our analysis of the angular and frequency dependence of the emissivity. This basic classification was kept for this specific application. The same classification is then applied to the multisatellite two-month data set (SSM/I, TMI, and AMSU), based on the SSM/I emissivity values.

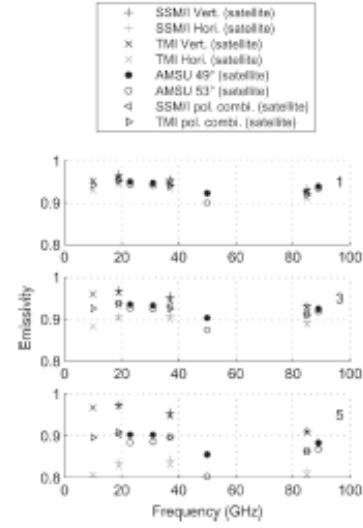


Fig. 4. Mean emissivity frequency dependence as observed from satellite-derived emissivities from the SSM/I, TMI, and AMSU-A around a 53° incidence angle for the three snow-free surface types. Both the vertical and horizontal polarizations are shown for the SSM/I and TMI. For AMSU-A, a polarization combination is measured, and for comparison, the same combination is calculated from the SSM/I and TMI perpendicular polarizations.

In the interpolation process, the emissivity of a specific location and month, for a given frequency, angle, and polarization, will be estimated from the actual emissivity of that location and month in the SSM/I-derived emissivity climatology, using the classification information only for the derivation of the frequency and angular dependences.

#### B. Frequency Dependence

**1) Analysis With the Satellite-Derived Emissivities:** The data set of two months of SSM/I, TMI, AMSU emissivities is sorted per surface types, using the SSM/I emissivity classification. For each snow-free class, Fig. 3(a) shows the frequency dependence of the SSM/I and TMI emissivity estimates in both polarizations, calculated from the satellite observations. The standard deviation over the class is indicated for the SSM/I estimates for each class. The results are shown for January 2003. The emissivities calculated from the satellite observations from SSM/I and TMI for the same frequencies agree very well for all the classes. The emissivities above 19 GHz have a very weak and close to linear frequency dependence, decreasing with frequencies, regardless of surface types. The TMI 21-GHz emissivity sticks out for all surface classes. It is likely related to an intercalibration problem. It could also be associated to a problem in the estimation of the absorption in the water vapor line, due to gaseous model errors or to errors in the water vapor profile estimates. This has not been elucidated. The 10-GHz emissivities are systematically and significantly lower than the 19-GHz ones, for both polarizations.

For the snow classes, Fig. 3(b) shows the frequency variation of the SSM/I emissivities (TMI does not cover the northern

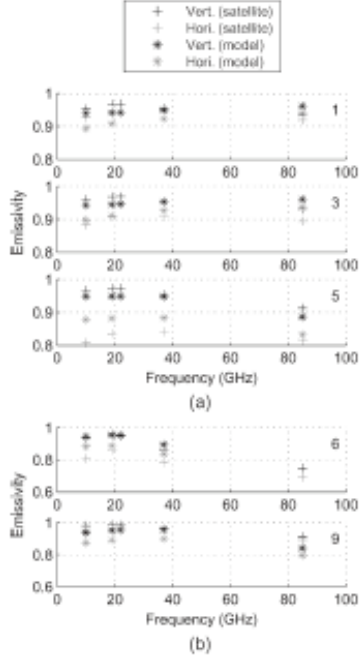


Fig. 5. Mean emissivity frequency dependence as observed from satellite-derived emissivities and from a model simulation at a  $53^\circ$  incidence angle, for both polarizations for January 2003, (a) for the snow-free surface types and (b) for the snow-covered surfaces. The satellite-derived estimates are from the SSM/I at 19 GHz and above and from TMI at 10 GHz. A limited number of classes are shown, the intermediate ones having an intermediate behavior. Note that the model values for the second snow type are out of the plotted range (lower values).

latitudes and, as a consequence, provides very limited snow-emissivity estimates). The emissivity decreases with frequency. The slope is stronger for class 6 which corresponds to the very cold regions where snow grains are likely large and can significantly scatter the microwave radiation. The higher the frequency, the stronger the scattering, thus explaining the decrease of the emissivities with frequency [20].

Fig. 4 compares the AMSU emissivities derived from the satellite observations to the SSM/I and TMI satellite-derived emissivities. The AMSU satellite emissivities over  $4^\circ$  around  $53^\circ$  are averaged for comparisons with TMI and SSM/I. In addition to the vertical and horizontal polarizations, the polarization combination that corresponds to the AMSU geometry is added. The satellite emissivity estimate at 50.3 GHz is obviously problematic, which is likely contaminated by error in the atmospheric correction (see [10] for additional comments on this problem). At low frequencies, the SSM/I- and TMI-derived emissivities are larger than the AMSU ones. However, above 80 GHz, the opposite prevails regardless of the surface type.

2) *Comparison With Model Estimates:* Fig. 5 compares the SSM/I emissivity estimates from the satellite observations and from the Weng *et al.* model [4]. The satellite estimates show a much larger polarization dependence than the model over arid and low-density vegetations [classes 5 and 4 on Fig. 5(a)], par-

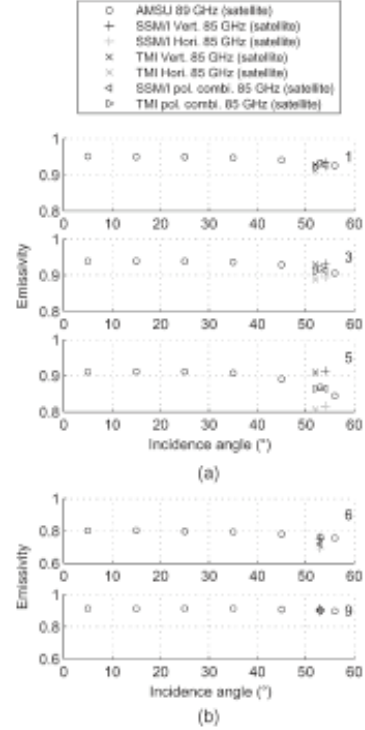


Fig. 6. Mean emissivity angular dependence as observed from satellite-derived emissivities from AMSU-A at 85 GHz, as compared to the SSM/I and TMI estimates at a  $53^\circ$  incidence angle in January 2003 (a) for three snow-free surface types and (b) for snow types.

ticularly at low frequencies. The following two reasons could explain it: the model can overestimate the roughness effect, or the assumed surface parameters are not adequate. Regardless of the surface type, the satellite-derived emissivities decrease with increasing frequency. Over the arid regions (class 5), the emissivities predicted by the model are rather stable with frequencies up to 40 GHz, and then decrease. Over the vegetated regions (classes from 1 to 3), the modeled emissivities increase with frequencies for the horizontal polarization. At 10 GHz with TMI, large differences are observed between the satellite estimates and the model, particularly for the horizontal polarization and over the arid regions.

For snow-covered regions, the differences between the satellite and model emissivities are significant but the trends in the frequencies are similar (note that the scales on the y-axis on Fig. 5(a) and (b) are different and that the model values for the snow type 6 at 85 GHz are lower than the plotted range).

### C. Angular Dependence

The analysis of the angular dependence of the satellite data can only be performed from the AMSU-A observations, i.e., not independently for each polarization.

The AMSU-satellite emissivities at 89 GHz are shown for different angles on Fig. 6, along with the SSM/I and TMI

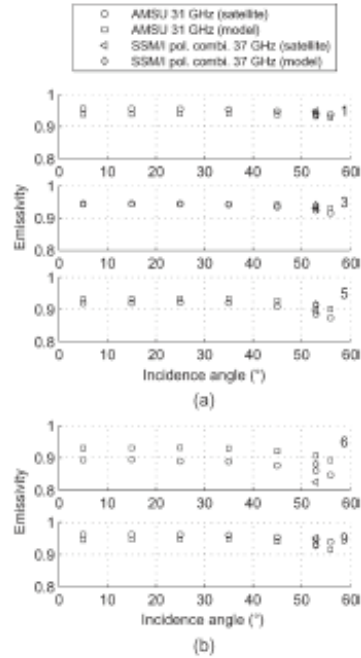


Fig. 7. Mean emissivity angular dependence as observed from satellite-derived emissivities from AMSU-A at 31 GHz and compared to the estimates at 37 GHz derived from SSM/I (a) for three snow-free surfaces and (b) for snow areas.

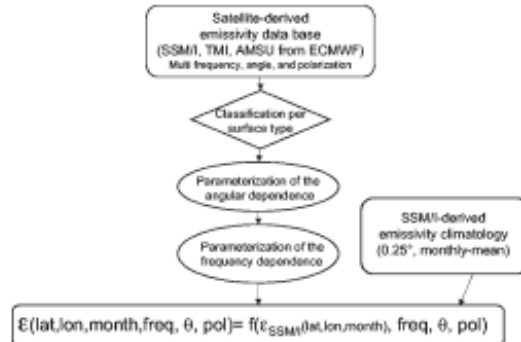


Fig. 8. Schematic presentation of the methodology.

satellite emissivities at 85 GHz. For all the surface types (snow-free and snow-covered regions), the angular dependence is smooth and limited: the polarization-combined AMSU emissivities are almost constant with the incidence angle up to 40° and then slightly decrease. The SSM/I- and TMI-derived emissivities around 53° at vertical and horizontal polarizations have been combined for comparison with the AMSU estimates. A rather good agreement is observed for all the surface types. Similar behaviors are seen at the other frequencies (not shown).

As compared to the model, the angular dependence of the satellite-derived emissivities is larger than the model ones

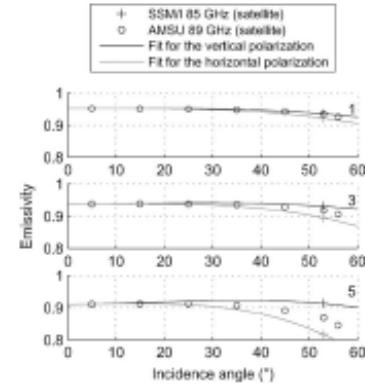


Fig. 9. Angular interpolation for each polarization, for three snow-free classes, as derived from the AMSU 89-GHz emissivities and anchored to the 85-GHz SSM/I emissivities.

(see Fig. 7 at 37 GHz; similar results are observed at the other frequencies). This is also related to the smaller polarization differences seen in the model than in the observation-derived emissivities.

#### IV. PARAMETERIZATION AND ITS RESULTS

Fig. 8 shows the methodology that is developed to derive the parameterization of the emissivity estimate for each location, month, frequency (between 19 and 100 GHz), incidence angle, and polarization. The development of the parameterization is based on the SSM/I and AMSU emissivity calculation performed at the ECMWF for January 2003, using only half the pixels for the snow-covered region. The method is then tested on the July 2002 emissivity calculations for the snow-free regions and on the remaining half of the January 2003 snow-covered pixels (as there is a very limited number of snow-covered pixels in July).

##### A. Parameterization of the Angular Dependence and Description of the Algorithm

**1) Parameterization of the Angular Dependence:** For each class that was previously defined, a polynomial function (third degree) is defined to describe the angular dependence of each polarization that fits both the SSM/I and AMSU-derived estimates. The polynomial function is calculated through a gradient descent to minimize the difference with the satellite-derived SSM/I and AMSU estimates. Fig. 9 shows the polynomial functions for three snow-free classes at 85 GHz, along with the corresponding satellite-derived emissivities from the SSM/I and AMSU.

**2) Description of the Algorithm:** The algorithm works as follows:

- 1) Selection of a location (latitude and longitude), month, frequency, and incidence angle. For a given location and month, a snow flag derived from the National Snow and Ice Data Center data is specified (snow or no snow).

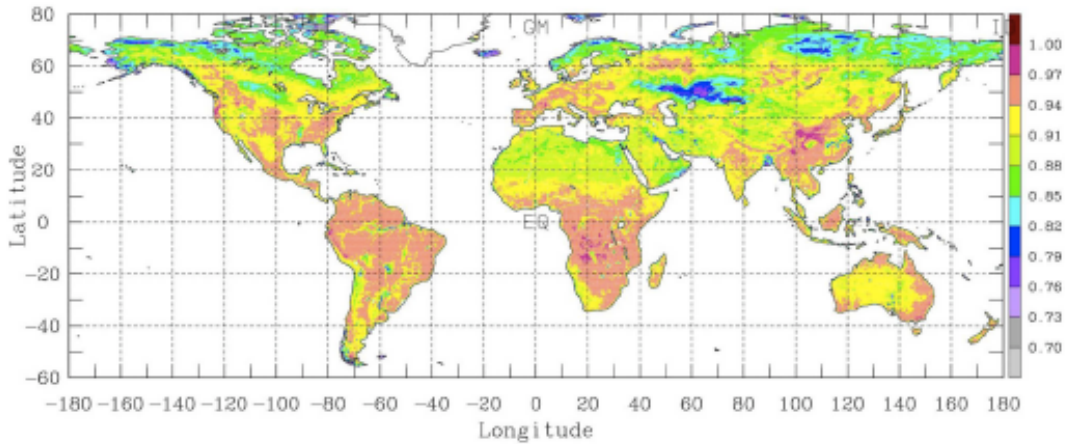


Fig. 10. Example of an emissivity map at 30 GHz, for a 40° incidence angle, horizontal polarization in February.

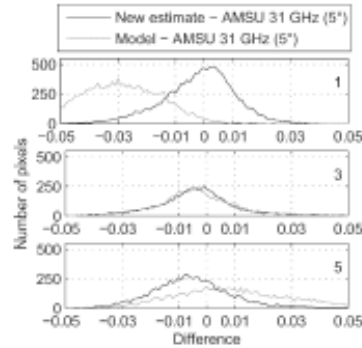


Fig. 11. Histogram of the differences between the new interpolated emissivity and the satellite-derived emissivity, along with the difference between the modeled emissivity and the satellite-derived emissivity, at 31.4 GHz, 5° incidence angle, for AMSU-A for three snow-free classes.

- 2) Search in the SSM/I climatology database for the emissivities for that given location and month. It gives  $e_v(53^\circ)$  and  $e_h(53^\circ)$  for the SSM/I frequencies at 19.35, 37.0, and 85.5 GHz.
- 3) For each frequency (19.35, 37.0, and 85.5 GHz), calculation of the corresponding emissivity at nadir [ $e_v(0^\circ)$  and  $e_h(0^\circ)$ ] from a multilinear regression of  $e_v(53^\circ)$  and  $e_h(53^\circ)$ . The coefficients of this multilinear regression have been calculated from each class, separately.
- 4) Application of the polynomial function that describes the angular dependence for each polarization and each SSM/I frequency to deduce the  $e_v(\theta)$  and  $e_h(\theta)$  emissivities.
- 5) Linear interpolation in frequency to derive  $e_v(\theta)$  and  $e_h(\theta)$  at the selected frequency from the three SSM/I frequency emissivity functions.

#### B. Results and Comparison With Other Estimates

Fig. 10 shows an example of parameterization at 30 GHz, at 40° incidence angle, horizontal polarization, for February.

The results of the parameterization are tested using the AMSU emissivities calculated at ECMWF for July 2002 and for half the pixels for January 2003 over snow. The ECMWF calculations are compared with both the parameterization results and the emissivity model outputs, which are also calculated at ECMWF (see Section II-B). The histograms of the differences for both estimates, at 31 GHz and 5° incidence angle, for the three snow-free classes are shown on Fig. 11. With the new parameterization over the snow-free regions, the differences are centered close to zero with a limited dispersion, regardless of the surface type. The behavior of the model is highly dependent on the surface type.

Table I summarizes the results of the comparison at 23, 31, and 89 GHz at 15° and 45° for each class. The bias is indicated, as well as the rms (in parentheses). Fig. 12 shows the rms error as a function of the surface class, for 15°, for both estimates.

For the snow-free regions, the new parameterization gives the rms values that are usually within 0.02, with a limited bias. Only a fraction of this error is directly related to the angular and frequency parameterization itself; the rest is due, first, to the temporal variabilities of the emissivities over a month and from year to year, and second, to the conditions of the calculation that were different at ECMWF and for the initial SSM/I emissivity climatology (Section II-A). The standard deviation of the emissivities within a month have been characterized [5] and are of the order of 0.01 at 19 GHz and can reach 0.02 at higher frequencies over snow (for the SSM/I emissivity database, these standard deviations are available along with monthly mean emissivities on our Web site geo.observ.fr). The gaseous absorption model, the surface skin temperature, and the cloud detection schemes are different in the calculations performed at the ECMWF and for the initial SSM/I emissivity climatology, inducing potential differences between the calculated emissivities; the sensitivity of the calculation to these various factors have already been evaluated [5]. For classes 2 and 3, the rms errors of the model are also almost always below 0.03.

TABLE I  
COMPARISON BETWEEN THE NEW PARAMETERIZATION AND THE SATELLITE-DERIVED EMISSIVITIES (A) AS WELL AS BETWEEN THE MODEL ESTIMATES AND THE SATELLITE-DERIVED EMISSIVITIES (B) AT 23, 31, AND 89 GHz AT 15° AND 45° FOR EACH CLASS. THE BIAS IS INDICATED, AS WELL AS THE RMS (BETWEEN PARENTHESES)

Class	15° 23GHz	45° 23GHz	15° 31GHz	45° 31GHz	15° 89GHz	45° 89GHz
1 (a)	-.003(.014)	.003(.015)	-.003(.013)	.001(.014)	.006(.016)	.006(.018)
1 (b)	-.034(.037)	-.028(.033)	-.025(.029)	-.020(.026)	.003(.015)	.009(.020)
2 (a)	-.006(.017)	.002(.018)	-.005(.016)	.000(.017)	.003(.018)	.005(.020)
2 (b)	-.024(.028)	-.017(.024)	-.016(.021)	-.010(.018)	.009(.018)	.017(.024)
3 (a)	-.003(.016)	.006(.018)	-.002(.015)	.004(.017)	.007(.017)	.010(.021)
3 (b)	-.010(.019)	-.002(.019)	-.002(.015)	.005(.019)	.020(.030)	.027(.037)
4 (a)	-.003(.018)	.007(.021)	-.002(.017)	.005(.020)	.009(.020)	.014(.027)
4 (b)	.003(.022)	.013(.029)	.010(.024)	.019(.031)	.017(.044)	.028(.054)
5 (a)	-.003(.019)	.012(.022)	-.003(.017)	.007(.019)	.010(.021)	.017(.030)
5 (b)	.009(.028)	.019(.032)	.012(.028)	.020(.032)	.033(.060)	.023(.062)
6 (a)	-.006(.039)	.008(.037)	.001(.047)	.010(.042)	.046(.070)	.051(.070)
6 (b)	.013(.047)	.024(.049)	.029(.052)	.040(.060)	.309(.402)	.308(.399)
7 (a)	-.005(.027)	.007(.029)	.009(.032)	.011(.033)	.036(.066)	.041(.068)
7 (b)	-.017(.031)	-.006(.028)	-.001(.032)	.008(.036)	.327(.415)	.328(.417)
8 (a)	-.001(.023)	.008(.027)	.003(.025)	.004(.030)	.005(.071)	.007(.071)
8 (b)	-.021(.031)	-.015(.029)	-.010(.029)	-.005(.031)	.180(.300)	.188(.309)
9 (a)	-.004(.019)	.003(.020)	-.003(.021)	-.000(.023)	-.004(.061)	.001(.062)
9 (b)	-.030(.034)	-.027(.032)	-.018(.026)	-.016(.025)	-.080(.166)	-.089(.179)

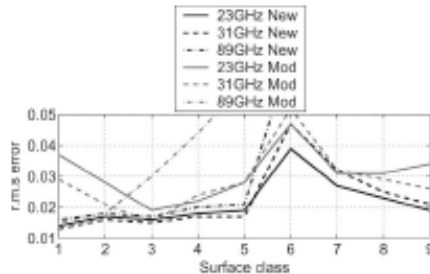


Fig. 12. RMS error between the new parameterization and the satellite-derived emissivities (black lines), as well as between the model estimates and the satellite-derived emissivities (gray lines) at 23, 31, and 89 GHz at 15° as a function of surface class.

For the snow-covered regions, much larger errors are observed, particularly at high frequencies for the snow classes that correspond to low emissivities (classes 6 and 7). In these regions, snow signatures are dominated by scattering, particularly at high frequencies, with a large temporal and spatial variability related to snow-grain metamorphism [20].

The emissivity model outputs have larger bias and rms for most cases. The ability of the model to represent the complexity of the radiation/surface interaction can be questioned. However, a large part of the error is likely related to the simplicity of the ECMWF surface model from which the emissivity model inputs are derived. This is particularly true over snow, where parameters like grain size distribution and stratification have a strong effect on the emissivity but are not available from the land surface models.

## V. CONCLUSION

The angular and frequency dependences of the microwave land surface emissivities are analyzed between 10 and 90 GHz from estimates derived from SSM/I, TMI, and AMSU and are compared to model calculations. For a given surface type, both

the angular and frequency dependences are rather limited and monotonic above 19 GHz. Below 19 GHz, the frequency dependence is different, and an additional work is to be performed, using Advanced Microwave Scanning Radiometer observations for instance. The general frequency and angular behaviors are rather similar, from models and satellite-derived emissivities, but differences in emissivities can be more than 10%.

From the analysis of the satellite-derived frequency and angular dependences, a parameterization is developed to estimate global microwave emissivities from the 19 to 100 GHz range for all the incidence angles and for both polarizations. It is anchored to a monthly mean emissivity climatology derived from the SSM/I observations for over a decade. The results are compared with model outputs and satellite estimates. The rms error is expected to be lower than 0.02 in snow-free region. The parameterization algorithm is available to the community, as well as the monthly mean emissivity climatology which it requires as inputs. The covariance of the emissivities from the original SSM/I-derived database is also accessible.

The uses of these emissivities are manifold as follows:

- 1) estimate the surface contribution in a cloud-clearing procedure;
- 2) as the first guess in the assimilation of close-to-the-surface sounding channels;
- 3) as the first guess in surface skin temperature retrievals using microwave observations for an "all-weather" estimate of the surface temperature to complement the infrared estimates that are only available under clear-sky condition;
- 4) evaluate the surface background contribution in precipitation and cloud retrievals;
- 5) simulate the responses of future instruments.

Efforts have to be conducted in collaboration with the land surface and emissivity modelers to better understand the differences observed between the satellite-derived and modeled emissivities. That will lead to the development of reliable and accurate emissivity models for global applications.

## ACKNOWLEDGMENT

Calculations of the AMSU, SSM/I, TMI emissivities for the two months were performed by F. Chevallier when he was at ECMWF in the Jean-Noel Thépaut Group, and the SSM/I emissivity climatology has been calculated in collaboration with B. Rossow at the NASA Goddard Institute for Space Studies. The authors would like to thank F. Weng and B. Yan (NOAA) for providing them with their model. The authors would also like to thank two anonymous reviewers and the guest editor for their helpful comments on the manuscript.

## REFERENCES

- [1] C. Matzler, "Passive microwave signatures of landscapes in winter," *Meteor. Atmos. Phys.*, vol. 54, no. 1–4, pp. 241–260, Mar. 1994.
- [2] T. J. Hewison, "Airborne measurements of forest and agricultural land surface emissivity at millimeter wavelengths," *IEEE Trans. Geosci. Remote Sens.*, vol. 39, no. 2, pp. 393–399, Feb. 2001.
- [3] J. Shi, K. S. Chen, Q. Li, T. J. Jackson, and P. E. O'Neil, "A parameterized surface reflectivity model and estimation of bare-surface soil moisture with L-band radiometer," *IEEE Trans. Geosci. Remote Sens.*, vol. 40, no. 12, pp. 2674–2686, Dec. 2002.
- [4] F. Weng, B. Yan, and N. C. Grody, "A microwave land emissivity model," *J. Geophys. Res.*, vol. 106, no. D17, pp. 20115–20123, 2001.
- [5] C. Prigent, W. B. Rossow, and E. Matthews, "Microwave land surface emissivities estimated from SSM/I observations," *J. Geophys. Res.*, vol. 102, no. D18, pp. 21 867–21 890, 1997.
- [6] F. Karbou, C. Prigent, L. Eymard, and J. Pardo, "Microwave land emissivity calculations using AMSU measurements," *IEEE Trans. Geosci. Remote Sens.*, vol. 43, no. 5, pp. 948–959, May 2005.
- [7] C. Prigent, F. Aires, and W. B. Rossow, "Land surface microwave emissivities over the globe for a decade," *Bull. Amer. Meteorol. Soc.*, vol. 87, no. 11, pp. 1573–1584, Nov. 2006. DOI:10.1175/BAMS-87-11-1573.
- [8] T. Pellerin, J.-P. Wigneron, J.-C. Calvet, and P. Waldteufel, "Global soil moisture retrieval from a synthetic L-band brightness temperature data set," *J. Geophys. Res.*, vol. 108, no. D12, p. 4364, 2003. DOI:1.1029/2002JD003086.
- [9] A. Wiesmann, C. Fierz, and C. Matzler, "Simulation of microwave emission from physically modeled snowpacks," *Ann. Glaciol.*, vol. 31, no. 1, pp. 397–405, Jan. 2000.
- [10] C. Prigent, F. Chevallier, F. Karbou, P. Bauer, and G. Kelly, "AMSU—A land surface emissivity estimation for numerical weather prediction assimilation schemes," *J. Appl. Meteorol.*, vol. 44, no. 4, pp. 416–426, Apr. 2005.
- [11] J. P. Hollinger, J. L. Pierce, and G. A. Poe, "SSM/I instrument evaluation," *IEEE Trans. Geosci. Remote Sens.*, vol. 28, no. 5, pp. 781–790, Sep. 1990.
- [12] R. W. Saunders, "Note on the advanced microwave sounding unit," *Bull. Amer. Meteorol. Soc.*, vol. 74, pp. 2211–2212, 1993.
- [13] W. B. Rossow and R. A. Schiffer, "Advances in understanding clouds from ISCCP," *Bull. Amer. Meteorol. Soc.*, vol. 80, no. 11, pp. 2261–2287, Nov. 1999.
- [14] J. R. Eyre, "A fast radiative transfer model for satellite sounding systems," ECMWF, Reading, U.K., p. 1991, ECMWF Tech. Memo. 176.
- [15] R. Saunders, M. Matricardi, and P. Brunel, "An improved fast radiative transfer model for assimilation of satellite radiance observations," *Q. J. R. Meteorol. Soc.*, vol. 125, no. 556, pp. 1407–1425, Apr. 1999.
- [16] E. Kalnay *et al.*, "The NCEP/NCAR 40-year reanalysis project," *Bull. Amer. Meteorol. Soc.*, vol. 77, no. 3, pp. 437–470, Mar. 1996.
- [17] T. Kohonen, *Self-Organization and Associative Memory*. New York: Springer-Verlag, 1984.
- [18] C. Prigent, F. Aires, W. B. Rossow, and E. Matthews, "Joint characterization of vegetation by satellite observations from visible to microwave wavelength: A sensitivity analysis," *J. Geophys. Res.*, vol. 106, no. D18, pp. 20 665–20 685, 2001.
- [19] C. Prigent, F. Papa, F. Aires, W. B. Rossow, and E. Matthews, "Global inundation dynamics inferred from multiple satellite observations, 1993–2000," *J. Geophys. Res.*, vol. 112, D12107, 2007.
- [20] E. Cordisco, C. Prigent, and F. Aires, "Snow characterization at a global scale with passive microwave satellite observations," *J. Geophys. Res.*, vol. 111, no. D19, D19102, 2006. DOI:10.1029/2005JD006773.



**Catherine Prigent** received the Ph.D. degree in physics from Paris University, Paris, France, in 1988.

Since 1990, she has been a Researcher with the Laboratoire d'Etudes du Rayonnement et de la Matière en Astrophysique, Paris Observatory, Centre National de la Recherche Scientifique (CNRS), Paris, France. From 1995 to 2000, she was on leave from CNRS and worked at the NASA Goddard Institute for Space Studies, Columbia University, New York, NY. Her research interests focus on passive microwave remote sensing of the Earth. Her early work focused on the modeling of the sea surface emissivities at microwave wavelengths and the estimation of atmospheric parameters over the ocean from microwave measurements. Currently, her main interests include the calculation and analysis of microwave land surface emissivities, estimation of atmospheric and surface parameters over land from microwave observations, as well as multisatellite characterization of the land surface. She is also involved in satellite remote sensing of clouds with the analysis of passive-microwave observations over convective cloud structures.

**Elodie Jaumouillé** received the M.S. degree in applied mathematics from Bordeaux I University, Bordeaux, France, in 2005. She is currently working toward the Ph.D. degree in applied mathematics at Cemagref, Bordeaux.

She was with the Laboratoire des Sciences du Climat et de l'Environnement, Commissariat à l'Energie Atomique, Gif-Sur-Yvette Cedex, France, where she was involved in the numerical and scientific validation of several climate models' outputs. Then, she is with the Laboratoire d'Etudes du Rayonnement et de la Matière en Astrophysique, Paris Observatory, Paris, France. She studied the frequency and angular variations of microwave emissivities. She is investigating how to control the hydraulic state of a drinkable-water network in order to minimize losses and to assure a better quality for the customer.

**Frédéric Chevallier** received the M.S. degree in physics at the University of Rennes, Rennes, France, in 1993. His Ph.D. work, which he defended in 1998, consisted of the development of a neural-network-based infrared radiation model for use in general circulation models. This study took place at the Laboratoire de Météorologie Dynamique, Palaiseau Cedex, France.

In 1998, he was with the European Centre for Medium Range Weather Forecasts, Reading, U.K., to work in the physical aspects and satellite sections. There he adapted his radiation model, which was made operational in 2003 as part of the 4-D-Var physics. His involvement in the data assimilation system increased over the years, particularly in initiating the assimilation of cloud-affected and rain-affected satellite radiances. He was appointed as a Permanent Research Scientist with the Laboratoire des Sciences du Climat et de l'Environnement, Gif-Sur-Yvette Cedex, France, in December 2003. His current research interests focus on the Bayesian inversion of the surface fluxes of atmospheric compounds from *in situ* and remote sensing atmospheric measurements.

**Filipe Aires** received the Ph.D. degree in statistics from the University Paris-Dauphine, Paris, France, in 1999.

He was with the NASA Goddard Institute for Space Studies, New York, NY, for five years, and he is now a Research Scientist with the Laboratoire de Météorologie Dynamique, Centre National de la Recherche Scientifique, Palaiseau Cedex, France. His research interests focus on satellite remote sensing of the Earth and statistical analysis of the climate. In earlier works, he analyzed climatic signals, using statistical techniques such as independent component analysis. He has also defined new tools for the characterization of climate feedback. He has developed multiinstrument and multiparameter remote sensing algorithms to retrieve atmospheric variables such as temperature, ozone, or water vapor profiles, and surface variables such as surface skin temperature, vegetation indices, or microwave emissivities. Instruments involved in these remote sensing studies include Advanced Microwave Sounder Unit, Special Sensor MicrowaveImager, Infrared Atmospheric Sounding Interferometer, European Remote-Sensing, and TIROS Operational Vertical Sounder. Currently, he is involved in the development of remote sensing algorithms for the French-Indian mission Megha-Tropiques.

## Annexe 4: Paper Aires et al., 2011.

Quarterly Journal of the Royal Meteorological Society

*Q. J. R. Meteorol. Soc.* (2011)



### A Tool to Estimate Land-Surface Emissivities at Microwave frequencies (TELSEM) for use in numerical weather prediction

Filipe Aires,<sup>a,b\*</sup>† Catherine Prigent,<sup>b</sup> Frédéric Bernardo,<sup>a</sup> Carlos Jiménez,<sup>b</sup> Roger Saunders<sup>c‡</sup> and Pascal Brunel<sup>d</sup>

<sup>a</sup>Laboratoire de Météorologie Dynamique/IPSL/CNRS, Université de Paris VI/Jussieu, Paris, France

<sup>b</sup>Laboratoire de l'Etude du Rayonnement et de la Matière en Astrophysique, CNRS, Observatoire de Paris, Paris, France

<sup>c</sup>Met Office, Exeter, UK

<sup>d</sup>Météo-France, Lannion, France

\*Correspondence to: F. Aires, CNRS/IPSL/Laboratoire de Météorologie Dynamique, Université Pierre et Marie Curie, case 99, 4 place Jussieu, F-75252 Paris Cedex 05, France. E-mail: filipe.aires@lmd.jussieu.fr

†Now at Estellus, France.

‡ The contribution of these authors was written in the course of their employment at the Met Office, UK, and is published with the permission of the Controller of HMSO and the Queen's Printer for Scotland.

A Tool to Estimate Land Surface Emissivities at Microwave frequencies (TELSEM) has been developed for use with the Radiative Transfer for the Television and infrared Observation satellite operational Vertical Sounder (RTTOV) model. Its objective is to provide a good estimate of the microwave surface emissivity to improve the retrieval of atmospheric profiles or the direct assimilation of radiances in numerical weather prediction (NWP) models using microwave sounder data over land. TELSEM provides emissivity estimates and error-covariance matrices for all land surfaces between 19 and 100 GHz and for all angles and linear polarizations. It is based on a pre-calculated monthly-mean emissivity climatology derived from Special Sensor Microwave/Imager (SSM/I) observations. Results show that when TELSEM is used, radiative-transfer simulations are closer to real observations. This is important when RTTOV is used to generate simulated datasets, to analyze new instrument concepts or for assimilation schemes. Experiments also show that TELSEM can be applied to provide a first guess for the surface emissivity down to 6 GHz and up to 190 GHz (extrapolating the SSM/I emissivities). These emissivities are essential for atmospheric profile retrievals over land: results for water-vapour retrieval show that surface-contaminated channels can be utilized and that the retrieval is improved, in particular for the lower troposphere. Furthermore, TELSEM emissivity first guesses can be improved in emissivity-retrieval schemes. Copyright © 2011 Royal Meteorological Society and British Crown Copyright, the Met Office

**Key Words:** remote sensing; assimilation; radiative transfer; water vapour

Received 9 August 2010; Revised 20 November 2010; Accepted 6 February 2011; Published online in Wiley Online Library

Citation: Aires F, Prigent C, Bernardo F, Jiménez C, Saunders R, Brunel P. 2011. A Tool to Estimate Land-Surface Emissivities at Microwave frequencies (TELSEM) for use in numerical weather prediction. *Q. J. R. Meteorol. Soc.* DOI:10.1002/qj.803

#### 1. Introduction

Surface-sensitive microwave observations from satellite instruments contain key information about lower-troposphere temperature and water vapour, cloud liquid water and precipitating water. Accurate estimates of

microwave land-surface emissivities are essential to extract such information in any inversion scheme such as statistical or 1D-Var retrievals or within complex 4D data assimilation system used in numerical weather prediction (NWP) centres. However, surface-sensitive microwave observations have been mainly used over the ocean. Over land, the surface

emissivity is complex to obtain from modelling, being spatially very variable and dependent upon a large number of parameters (e.g. soil moisture, vegetation, snow cover). They are also difficult to estimate from satellite observations: they are usually higher (close to unity, compared with low ocean emissivities), limiting the contrast with the atmospheric contribution. However, recent attempts have been made over continental regions to use<sup>†</sup> surface emissivities estimated from satellite observations (Aires *et al.*, 2001; Karbou *et al.*, 2005a).

In order to retrieve the surface emissivities and/or to perform satellite retrievals over land, various techniques can be used: direct estimation from satellite observations if only emissivity retrieval is necessary (Prigent *et al.*, 1997), statistical retrievals (Aires *et al.*, 2001) or ID-Var assimilation in NWP in order to perform multiple retrievals simultaneously (i.e. surface plus atmospheric retrievals). Most of them require a good (i.e. close enough to the true state) emissivity first guess (FG) that is refined during the inversion process (Aires *et al.*, 2001). In order to avoid ‘incest’ problems, this FG should be independent of the satellite observations used in the retrieval. A pre-calculated monthly-mean emissivity climatology can be used, but the FG needs to be as close as possible to the real emissivities, in particular taking into account not only the location and season but also the angle, frequency and polarization dependencies.

Land-surface emissivity models have been developed for various surface conditions over the globe (Weng *et al.*, 2001; Pellerin *et al.*, 2003), but they require a large number of input parameters that are not easily available such as soil composition, soil moisture, vegetation and snow characteristics. In parallel, global land surface emissivity datasets have been produced directly from satellite observations using Special Sensor Microwave/Imager (SSM/I) measurements (Prigent *et al.*, 1997; 2006) or, using the same methodology, from the Advanced Microwave Sounding Units (AMSU) (Prigent *et al.*, 2005a; Karbou *et al.*, 2005b). These estimations are made under clear-sky conditions. The principle is simple: the signal that is measured by the satellite instrument is the sum of two terms, one related to the surface and one to the atmosphere. If the atmospheric term can be estimated, the term associated with the surface can then be easily inferred. The International Satellite Cloud Climatology Project (ISCCP) (Rossow and Schiffer, 1999) provides cloud-flag information and ancillary data are used to estimate the atmospheric contribution. This approach can be difficult to implement directly in an atmospheric retrieval scheme for the following reasons.

- It requires a cloud-clearing procedure (NWP systems suffer from the quality of their cloud flag).
- An estimation of the atmospheric composition is necessary: this is easy to obtain in NWP centres (this can be the short-range forecast), but can be more complex for stand-alone retrieval schemes.
- It can be computationally demanding, since it requires the use of a radiative transfer code.

Furthermore, the emissivity estimates might not be robust for all types of configuration. For instance,

<sup>†</sup>In section 3.2 we show how to use these emissivities in a retrieval scheme.

for a given period of time, AMSU only provides a limited number of overpasses of the same location with the same incidence angle, and does not give access to the vertical and horizontal polarization information separately.

In a previous work (Prigent *et al.*, 2008), a parametrization of the land-surface emissivities between 19 and 100 GHz under all observing conditions has been derived. It is based on an analysis of the frequency, angular, and polarization dependences of the emissivities calculated from SSM/I, Tropical Rainfall Measuring Mission (TRMM) Microwave Instrument (TMI) and AMSU. We used this parametrization to develop the Tool to Estimate Land-Surface Emissivities at Microwave frequencies (TELSEM). This emissivity interpolator allows us to obtain an emissivity FG for each location over the globe and for any month of the year. Its range of frequencies is 19–100 GHz but we will show that it can be used in extrapolation mode for lower or higher frequencies. It can provide an emissivity FG for any incidence angle and polarization configuration. TELSEM has been implemented in the RTTOV model (Saunders *et al.*, 1999), to provide microwave radiance users with a robust estimation of the microwave emissivity over land. This new facility should be useful for radiative transfer studies, retrieval schemes or assimilation in NWP models. TELSEM is not intended to estimate emissivities based on the actual satellite observations; it provides a good FG independent of the satellite observations. TELSEM provides realistic emissivity uncertainties, estimated to be lower than 0.02 in snow-free regions, and also includes error-covariance matrices that include the reference climatology uncertainties and the emissivity interpolator errors.

Note that this microwave emissivity tool is generic and flexible: it can be interfaced with other radiative codes such as the Community Radiative Transfer Model (CRTM) developed by the Joint Center for Satellite Data Assimilation (JCSDA) (Weng *et al.*, 2005).

In section 2, the emissivity interpolation method is summarized and the reference surface-emissivity climatology from SSM/I observations is presented, along with the emissivity dataset from multiple instruments used to calibrate the interpolator. The interpolation principle and its implementation are commented on, and the uncertainty characterization is described. TELSEM is mainly designed to provide a FG to be improved in a retrieval scheme but the TELSEM emissivities can also directly be useful as a valuable emissivity estimation. Three applications of these estimates are presented in section 3. First, the impact of TELSEM on radiative-transfer simulations for AMSU-A and B instruments on board the National Oceanic and Atmospheric Administration (NOAA)-17 platform is measured. Second, results of atmospheric water-vapour retrievals over land are analyzed using Advanced Microwave Scanning Radiometer (AMSR)-E and Humidity Sounder for Brazil (HSB) observations, called hereafter ‘AQUA observations’. Third, the TELSEM emissivity estimate is then improved in a statistical retrieval scheme. Conclusions and perspectives are drawn in section 4.

## 2. The land-surface emissivity estimates, its associated errors, and its implementation in the radiative transfer code

### 2.1. The reference climatology

A monthly-mean emissivity database has been produced and analyzed for the 1993–2004 period from SSM/I measurements (Prigent *et al.*, 2006) by removing the contribution of atmosphere, clouds, rain and surface temperature, using ancillary data and radiative-transfer calculations. The emissivities are estimated from SSM/I observations, i.e. at 19.35, 22.235, 37.0, and 85.5 GHz, for both vertical and horizontal polarizations (with the exception of 22 GHz, which is vertical polarization only), with 53° incidence angle. They are available with a spatial resolution of 0.25° × 0.25° at the equator (equal-area grid). These emissivities have been thoroughly analyzed. They provide key information on the surface characteristics and have been used in numerous applications (Prigent *et al.*, 2001; 2007; Aires *et al.*, 2005; Jimenez *et al.*, 2009). A reference SSM/I-derived land-surface-emissivity climatology is derived from this dataset.

### 2.2. TELSEM calibration dataset

In order to derive general estimates of the emissivities, land-surface emissivities calculated at the European Centre for Medium-range Weather Forecasts (ECMWF) under a large range of frequencies, incidence angles and polarizations have been analyzed for SSM/I, TMI and AMSU-A observations for two months (July 2002 and January 2003) over the globe. TMI frequencies are similar to the SSM/I ones, with the addition of a lower frequency channel (10.65 GHz), for both polarizations. In addition to the O<sub>2</sub> sounding channels around 55 GHz, AMSU-A has window channels at 23.8, 31.4, 50.2 and 89 GHz. It is a cross-track scanning instrument, with 30 scan positions up to 58.5°. The polarization rotates with the scan angle due to the rotating-reflector/fixed-feed type of antenna design and is a known mix of vertical and horizontal polarizations. The emissivity calculation method follows closely the scheme previously developed for SSM/I (Prigent *et al.*, 2006). In the calculations performed at ECMWF, the selection of the clear pixels is based on the ECMWF forecast model and the atmospheric contribution is also calculated from the ECMWF forecast-model variables using RTTOV.

In order to facilitate the analysis of the frequency and angular dependences of the SSM/I, TMI and AMSU emissivities, the dataset is sorted per surface type, using a classification of the SSM/I emissivity itself based on the reference SSM/I emissivity dataset. This ensures that each class represents a different behaviour in terms of microwave emissivities and that the set of classes describes the full variability of these emissivities. The frequency and angular dependence of the satellite-derived emissivities are then analyzed for each surface type. Five surface types are identified for snow-free regions, from dense forest to deserts, and four snow types are isolated. The tenth class indicates pixels that contain standing water.

### 2.3. The emissivity parametrization

Analysis of this calibration dataset showed that the frequency, angular and polarization dependences are related to surface types but can be parametrized rather simply, with the SSM/I-derived monthly-mean emissivity climatology as a basis for the parametrization (Prigent *et al.*, 2008). For each surface type, the angular and frequency dependences are smooth enough to describe using simple polynomial functions, anchored to the SSM/I emissivity climatology.

The interpolator is composed of the following steps (see Figure 1).

- For the location (latitude and longitude) and month selected by the user, the algorithm searches for the corresponding SSM/I emissivity in the reference climatology. It gives  $Em_{SSMI}V(53^\circ)$  and  $Em_{SSMI}H(53^\circ)$ , i.e., the vertical and horizontal polarization emissivities at 53° incidence angle, for the SSM/I frequencies at 19.35, 37.0 and 85.5 GHz.
- Then for each SSM/I frequency (19.35, 37.0, 85.5 GHz), the algorithm calculates the corresponding emissivity at nadir  $EmV(0^\circ)$  (which equals  $EmH(0^\circ)$ ) from a multilinear regression of  $Em_{SSMI}V(53^\circ)$  and  $Em_{SSMI}H(53^\circ)$ . The coefficients of this multilinear regression have been pre-calculated for each class, separately.
- The next step consists of applying a pre-computed polynomial function that describes the angular dependence for each polarization and each SSM/I frequency to deduce the emissivities  $EmV(\theta^\circ)$  and  $EmH(\theta^\circ)$  at the incidence angle  $\theta$  selected by the user.
- Finally, a linear interpolation in frequency is applied to derive  $EmV(\theta^\circ)$  and  $EmH(\theta^\circ)$  at the user's selected frequency from the three SSM/I frequency emissivity functions.

It should be mentioned that a climatology has been used to define, in the reference-emissivity climatology, the location of snow-covered pixels. It is expected that the use of this snow climatology will bring problems during snowmelt/freezing because, for a particular date, the reality of the situation can be different from the climatology.

The validity of the regression coefficients is optimal for the 19–85 GHz frequency range of SSM/I. However, tests

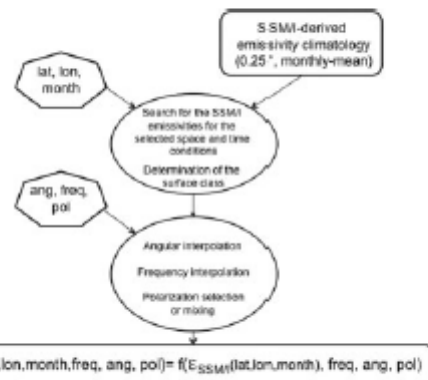


Figure 1. The different steps in TELSEM.

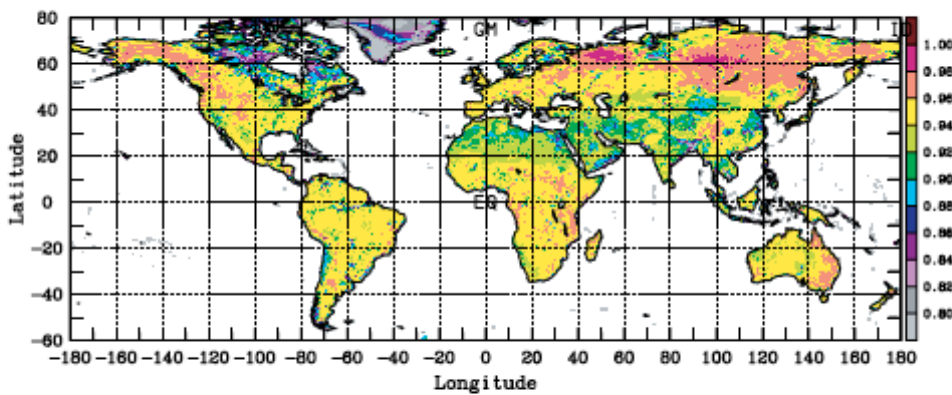


Figure 2. Example of emissivity calculation with TELSEM for September at 31.4 GHz (AMSSU-A channel), for 15° incidence angle and vertical polarization.

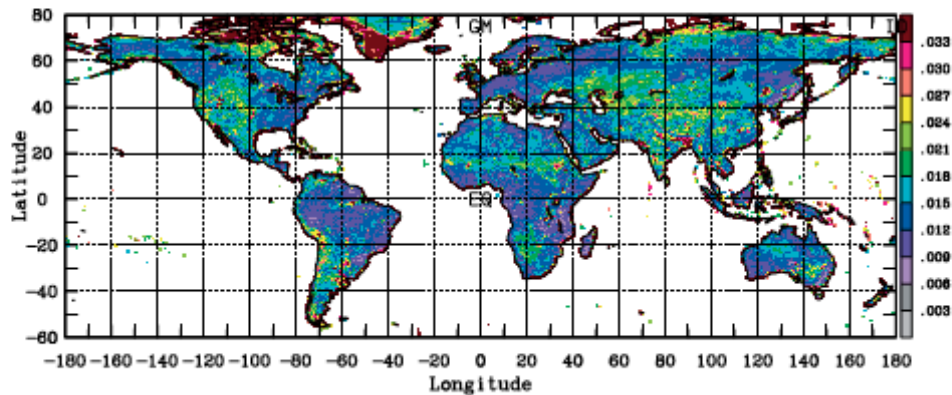


Figure 3. The emissivity uncertainty estimates for September, interpolated at 31.4 GHz (AMSSU-A channel), for the vertical polarization at 15° incidence angle.

show that TELSEM can be useful in frequency-extrapolation mode. For frequencies lower than 19 GHz, the 19 GHz emissivities are adopted. This has been evaluated down to 6 GHz (see section 3). For frequencies higher than 85 GHz, the 85 GHz emissivities are used. AMSSU-B emissivities at 150 GHz have been calculated directly from the satellite observations as described above. However, these calculations showed large variabilities related to water-vapour errors and cloud contamination<sup>1</sup> and tests proved that the use of the 85 GHz emissivity estimates was more reliable (Karbou et al., 2005b).

Figure 2 shows an example of emissivity interpolation for September at 31.4 GHz, for a 15° incidence angle and vertical polarization (i.e. quite different conditions compared with the reference climatology that is used, with SSM/I channel frequencies and a constant incidence angle of 53°). The interpolation scheme preserves the spatial structure of the microwave emissivities, for instance the

hydrological features in South America or the geologically related information in the North African desert (Prigent et al., 2005b). More details on the parametrization and its evaluation are provided in Prigent et al. (2008).

#### 2.4. Estimation of the error-covariance matrices of the interpolated emissivities

For most applications the errors associated with the emissivities have to be evaluated, as this information is essential for most retrieval scheme, especially in assimilation systems. When emissivities under several conditions (at different frequencies or polarizations for instance) are used together, the covariance matrix of these errors also needs to be estimated.

An error budget has been estimated for the reference SSM/I-derived emissivities taking into account the various sources of errors in the calculation (Prigent et al., 1997): the accuracy of the instantaneous retrieved emissivities is estimated to be within 1–2%. At monthly mean scales, the standard deviation of the emissivity calculation for each frequency is considered as a measure of the error. Careful analysis and comparisons with other emissivity products

<sup>1</sup>A rather old version of the ECMWF model has been used here and improvements in the quality of the ECMWF analysis/forecast are likely to improve the results.

## TELSEM Microwave Emissivities

Table I. The correlation matrix for uncertainties in the reference SSM/I emissivity climatology for forested regions (class 1).

SSM/I Channels	19V	19H	22V	37V	37H	85V	85H
19 GHz V	1.00	0.96	0.92	0.96	0.94	0.72	0.73
19 GHz H	0.96	1.00	0.90	0.95	0.95	0.71	0.72
22 GHz V	0.92	0.90	1.00	0.92	0.91	0.78	0.78
37 GHz V	0.96	0.95	0.92	1.00	0.96	0.79	0.79
37 GHz H	0.94	0.95	0.91	0.96	1.00	0.76	0.78
85 GHz V	0.72	0.71	0.78	0.79	0.76	1.00	0.93
85 GHz H	0.73	0.72	0.78	0.79	0.78	0.93	1.00

validated this approach. The challenge is now to adjust these SSM/I emissivity errors for the new interpolated emissivities.

Let  $Em_{SSMI}(6)$  be the six-channel SSM/I emissivities from the reference climatology for the 19V, 19H, 37V, 37H, 85V and 85H channels. The SSM/I reference-emissivity climatology also provides the  $6 \times 6$  correlation matrix,  $Cor_{SSMI}(6, 6)$ , for the uncertainties for the 6 SSM/I channels together with the associated uncertainty standard-deviation vector,  $Std_{SSMI}(6)$ . The covariance matrix of the SSM/I emissivity uncertainties can easily be estimated using

$$Cov_{SSMI} = Std_{SSMI}^T \cdot Cor_{SSMI} \cdot Std_{SSMI} \quad (1)$$

where  $T$  denotes the transpose of the matrix. A study has been conducted using the reference climatology to measure the variability of the correlation of errors for all pixels on a particular surface type. It appears (not shown) that the matrices  $Cor_{SSMI}$  are quite robust: for a particular surface type, the standard deviations of the correlations are small compared with the actual correlation. This means that, for each of the ten surface types, a unique error-correlation matrix  $Cor_{SSMI}$  can be estimated and then used. An example of such a correlation matrix is given in Table I for class 1 (i.e. highly vegetated areas). The structure of this matrix is complex for each vegetation class and it varies from one class to another. The correlations between channels are highly significant and cannot be neglected. In particular, it is important to use this correlation structure in a variational assimilation experiment and in all inversion schemes in general. If the covariance-error matrix is assumed diagonal (i.e. only the standard deviations of errors are accounted for), the uncertainties are underestimated. The fact that a single correlation matrix is used for all situations for a given surface type is a simplification that allows for a faster use of the interpolator, without any significant loss of accuracy. Note that the  $Cor_{SSMI}$  correlation matrix is constant for each surface type but the  $Std_{SSMI}$  standard-deviation matrix in the SSM/I emissivity climatology is provided by the interpolator, so that each spatial location over land will have a different  $Cov_{SSMI}$  covariance matrix (Eq. (1)).

The goal of the emissivity interpolator is to estimate new emissivities  $Em_{NEW}(f)$ , where  $f$  is the number of new frequencies to be calculated by the interpolator (at different scanning angles and polarizations). The first half of  $Em_{NEW}$  is for the vertical polarizations and the second half for the horizontal ones (this is the way it was implemented in the TELSEM code). The emissivity parametrization described in section 2.3 allows for the estimation of  $Em_{NEW}(f)$  using a  $(f \times 6)$  matrix,  $A$ , such that

$$(Em_V; Em_H) = A \cdot Em_{SSMI}. \quad (2)$$

The difficulty is then to make a realistic assessment of the errors of the interpolated emissivities. Simple algebra shows that the covariance matrix of the new emissivity uncertainties can be estimated by

$$\begin{aligned} Cov_{NEW} &= A^T \cdot Cov_{SSMI} \cdot A \\ &= A^T \cdot Std_{SSMI}^T \cdot Cor_{SSMI} \cdot Std_{SSMI} \cdot A. \end{aligned} \quad (3)$$

As a consequence, TELSEM not only provides a set of emissivities at new frequencies, angles and polarizations, but also estimates the full covariance matrix for this new set of channels.

In summary, the standard-deviation matrix  $Std_{SSMI}$  and the corresponding correlation matrix  $Cor_{SSMI}$  are provided by the reference-emissivity climatology. The interpolator calculates the new covariance matrix  $Cov_{NEW}$  for each location over land, and for each month, for the frequencies specified by the user. Figure 3 provides the uncertainty estimates interpolated at 31.4 GHz for the vertical polarization at  $15^\circ$  incidence angle for September (associated with the emissivity estimates of Figure 2). As expected, large uncertainties are related to temporally variable features such as wetlands (e.g. over Bangladesh) or snow- or ice-covered regions (e.g. over Greenland).

### 2.5. Implementation of the emissivity module in the RTTOV code

The RTTOV model has been developed for very rapid calculations of radiances in the infrared and microwave, primarily for use in variational assimilation of satellite observations within NWP centres (Saunders *et al.*, 1999). It was jointly developed by the Met Office (UK), Météo-France and ECMWF in the framework of the EUMETSAT-funded NWP Satellite Application Facility and also other EUMETSAT sponsored activities. The original code was described by Eyre and Woolf (1988). Matricardi *et al.* (2004) presents more recent developments. It is a compromise between calculation accuracy and speed. The absorption models are parametrized to produce regressions as a function of a selection of model predictors such as temperature and humidity, based on training datasets of accurate line-by-line absorption models and representative atmospheric-profile aspects. RTTOV-9 was released in 2008 and computes sea-surface emissivity as a function of surface wind speed, using the FASTEM-3 code developed by Deblonde and English (2001).<sup>§</sup> However, it does not provide accurate estimates

<sup>§</sup>See [http://www.metoffice.com/research/interproj/nwpsaf/rtrm/rttov8\\_svr.pdf](http://www.metoffice.com/research/interproj/nwpsaf/rtrm/rttov8_svr.pdf).

of the land-surface emissivity: a fixed microwave surface-emissivity value is suggested for each channel (English and Hewison, 1998), regardless of the observing conditions (the impact of such a simplification will be measured in section 3 and in Figure 4).

The TELSEM parametrization has been added as a new tool to the RTTOV simulator. The only information to be provided by the user is the geographical location (latitude and longitude) and the month. The nominal spatial resolution of the emissivity estimates is  $0.25^\circ \times 0.25^\circ$  but, if desired, the user can specify another spatial resolution (always degraded compared with the initial one): the code can use the closest climatology-derived emissivity or it will perform spatial averaging. The calculation can be performed individually for single frequency channels but also for multiple channels, in which case error-covariance matrices are provided. TELSEM simulations are very fast. However, it is recommended that TELSEM users interested in a particular instrument generate once and for all their own reference-emissivity climatology at the relevant horizontal resolution. This new reference climatology can then be used as a convenient FG or a simple emissivity estimate.

### 3. Impact of TELSEM on forward and inverse radiative transfer

TELSEM emissivities are not regular emissivity estimates, rather they are a FG climatology that can be used for many different instruments and various observing conditions. In this section, we measure the impact of this tool on radiative-transfer simulations and on atmospheric retrievals over land.

#### 3.1. Comparison with AMSU-A and -B observations on board NOAA-17

In order to evaluate TELSEM emissivities, RTTOV radiative-transfer calculations have been performed with and without the new tool and compared with satellite observations. Comparisons are also performed using emissivities simulated at ECMWF with the radiative-transfer model from Weng *et al.* (2001). The inputs for these model-based emissivity calculations are provided by the forecast model (e.g. soil temperature and humidity, vegetation fraction or snow characteristics). This model uses different solutions depending on the surface type.

For this experiment, observations from NOAA-17 are collected for July 2002 and January 2003, in order to sample the seasonal cycle. The observations from the AMSU-A and -B cross-track sounders are first collocated. The atmospheric profiles and relevant surface parameters are extracted from the ECMWF analysis in order to have all the required information needed to perform radiative-transfer simulations. High-elevation locations ( $>1000$  m), precipitating scenes and high-latitude points ( $\text{lat} > 60^\circ$ ) are suppressed from the statistics. All incidence angles are included in these statistics.

Figure 4 compares the simulated and observed brightness temperatures (TBs): the two upper graphs are for bias statistics, while the bottom graphs are for the root-mean-square (RMS) differences. Left (resp. right) graphs are for clear (resp. cloudy) situations. Simulations are performed with TELSEM emissivities, with a constant emissivity

corresponding to the default RTTOV model and with the Weng *et al.* (2001) model. All these statistics are for continental surfaces but, for comparison purposes, the simulations have been performed over the ocean as well, with emissivities calculated with the FASTEM model (Deblonde and English, 2001).

The results are clearly better with the new TELSEM land-surface emissivities, and are similarly good for clear and cloudy scenes in term of both bias and RMS error statistics.

As expected, the stand-alone RTTOV constant emissivity introduces high bias errors on surface-sensitive channels. These large errors dominate the corresponding RMS errors. When the new TELSEM emissivities are used, these biases are reduced very significantly, close to zero. This reduction of the bias when using TELSEM has an important impact on the RMS statistics, with errors reduced by a factor of 3–4 for window channels. With TELSEM, RMS errors are always lower than with the stand-alone RTTOV emissivity or with the model-based calculations (model-based emissivities are highly dependent on the quality of the inputs of the model such as soil moisture or vegetation, which is a difficulty with this approach). As expected, there is no impact of the emissivity changes for opaque channels around 183 GHz or temperature-sounding channels. No bias correction procedure<sup>1</sup> is used for these comparison statistics, explaining part of the remaining differences.

Furthermore, the agreement between simulations and observations obtained with the new TELSEM surface emissivities is, for most channels, better than the one obtained over the ocean with FASTEM. Note that the fact that the RMS errors over ocean are larger than over land is likely not exclusively related to emissivity problems, but to the higher sensitivity to water vapour and clouds over the ocean. At 157 GHz, the 85 GHz emissivity is adopted in TELSEM: the effect is not large compared with the stand-alone RTTOV or the Weng model but is still positive, showing that this rather crude extrapolation is still beneficial. At this frequency and higher, the RMS error between the simulations and the observations is driven by the atmospheric components, with very similar behaviour over land and ocean for both clear and cloudy situations.

Land and ocean statistics being similar, even for surface-sensitive channels, means that the introduction of realistic microwave emissivities increases the accuracy of the forward radiative-transfer simulations. As a consequence, the accuracy of the retrieval of atmospheric parameters over land should be improved.<sup>2</sup>

#### 3.2. Impact of the land-surface emissivity in the inversion of atmospheric profiles

A French–Indian satellite mission, Megha-Tropiques, will be launched in 2011 (Desbois *et al.*, 2007). Its objective is to study the water cycle in the Tropics, with a high temporal sampling. Megha-Tropiques will carry two microwave instruments: a conical imager, Madras, with frequencies at 18.7, 23.8, 36.5, 89 and 157 GHz for both linear polarizations,

<sup>1</sup>The use of real observations in a remote-sensing code generally requires some bias tuning of the data so that the RTM simulations are close enough to the real observations (Aires *et al.*, 2010).

<sup>2</sup>Of course, given the brightness-temperature surface/atmosphere contrasts, retrievals are expected to be easier over ocean.

## TELSEM Microwave Emissivities

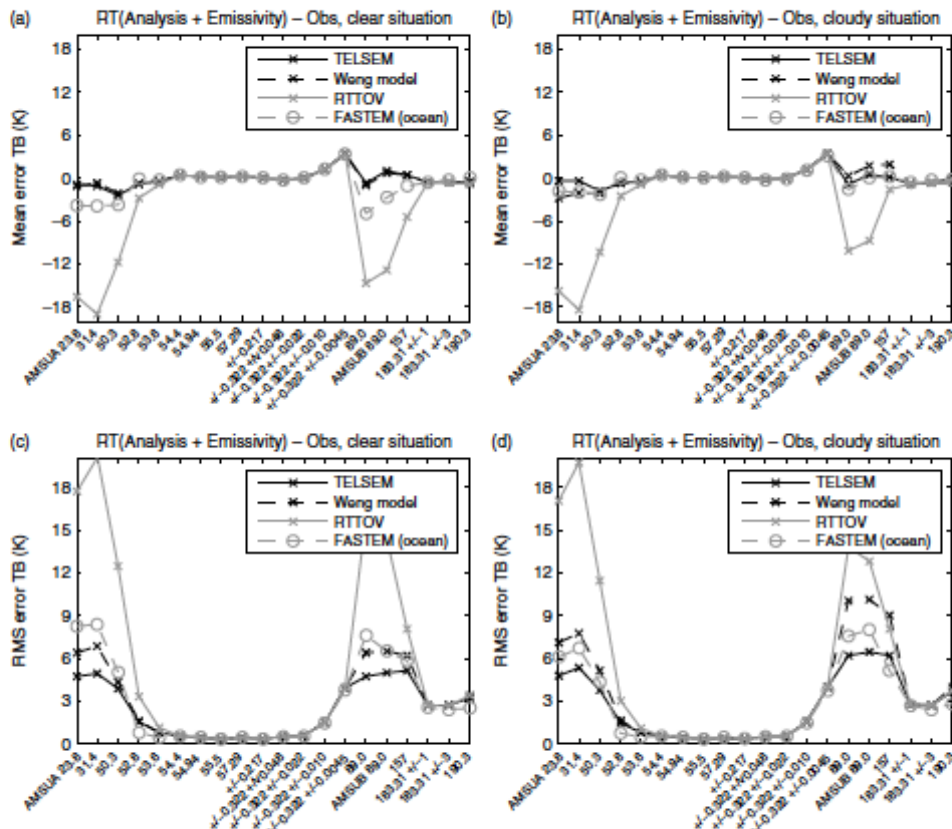


**Figure 4.** RMS errors between simulated and observed TBs for AMSU-A and AMSU-B on board NOAA-17, for two months (July 2002 and January 2003). High latitudes ( $\pm 60^\circ$  in latitude) and precipitating scenes have been excluded from the statistics. (a) Bias statistics for cloud-free situations, (b) bias for cloudy situations, (c) RMS statistics for cloud-free situations, (d) RMS for cloudy situations. The continuous black line denotes the simulations with the TELSEM emissivities, the continuous grey line the original RTTOV simulations using a fixed emissivity from a stand-alone RTTOV and the dashed black line emissivities from the Weng model. For comparison purposes, similar statistics are performed over the ocean using the FASTEM emissivity model, shown as the dashed/circle grey line.

and a cross-track humidity sounder, Saphir, with six channels around the 183 GHz water-vapour line. A neural network inversion has been developed to derive, among other variables, the water-vapour atmospheric profiles from the combination of the Madras and Saphir observations. The statistical method is trained on a simulated database using a global collection of ECMWF analysis coupled to the RTTOV radiative-transfer model. The operational inversion algorithm uses the new RTTOV tool to estimate the emissivities over land.

In order to evaluate the operational chain, tests have been conducted on existing satellite data at similar frequencies, using AMSR-E and HSB observations from AQUA, over the Tropics ( $\pm 30^\circ$ ) for two months (July 2002 and January 2003). Tests have been performed both in the forward and inverse modes. In the forward mode, similarly to Figure 4, the RMS errors between simulated and observed TBs are significantly better with TELSEM than with the fixed RTTOV emissivities, even at the lower AMSR-E frequency channels 6.925 and 10.65 GHz, where the

TELSEM emissivities at 19 GHz are adopted: for horizontal polarization channels, the RMS errors decrease from close to 30 K with RTTOV emissivities to around 10 K (the impact for vertical polarization channels is limited, with RMS errors around 6 K).

Figure 5 shows the RMS errors (or departures) for the retrieval of the relative humidity, calculated from the difference between the satellite retrieval and the analysis from ECMWF, assuming that the ECMWF analysis is the truth. For both clear and cloudy atmospheres, the results show that the retrieval accuracies for the lower layers below 750 hPa are of the same order (around 10–20% in RMS) over land and ocean. This is very encouraging. So far, observations from surface-sensitive channels over land have been disregarded. These results suggest that the use of realistic emissivity estimates can considerably increase the number of satellite observations to be assimilated over land, and provides estimates of atmospheric profiles in the lower layers over land with accuracies that are comparable to the accuracies over the ocean.

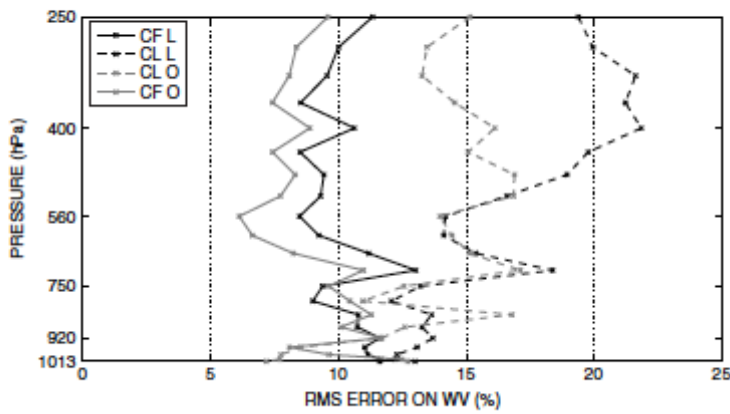
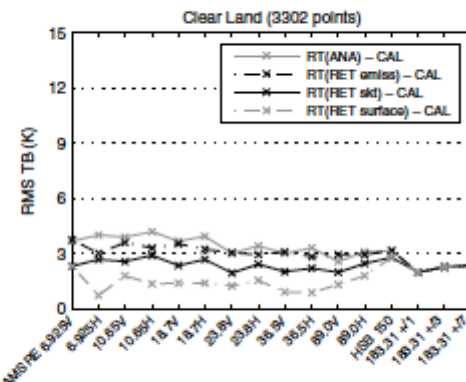


Figure 5. RMS relative error for the AMSR-E/HSB retrieval of relative humidity (in %). The statistics are given over the tropical regions ( $\pm 30^\circ$ ) for July 2002 and January 2003. Grey lines are for ocean surfaces (O) and black lines for land (L). Continuous lines are for cloud-free (CF) scenes and dashed lines are for cloudy (CL) situations.



**Figure 6.** RMS errors between simulated and observed TBs for AMSR-E and HSB instruments on board AQUA, for two months (July 2002 and January 2003). High latitudes ( $\pm 60^{\circ}$  in latitude), cloudy and precipitating scenes have been excluded from the statistics. RTTOV simulations use the following surface conditions: continuous grey line, FG information (TELSEM emissivities and TS from analysis); dashed black line, NN inverted emissivities only; continuous black line, TELSEM emissivities but NN  $T_s$  retrieval; dashed grey line, both surface emissivities and skin temperature from the NN retrieval.

### 3.3. Retrieval of the land-surface emissivity using TELSEM first guesses

In this section, the TELSEM emissivities are used as FG in a retrieval scheme that simultaneously inverts the surface skin temperature and emissivities. Similarly to section 3.2, the satellite observations come from the AMSR-E and HSB instruments on board the AQUA platform. The retrieval approach is similar to that used in Aires *et al.* (2001): a neural network (NN) uses as inputs a mix of information composed of the actual satellite observations plus a FG of both emissivities and surface skin temperature. The outputs are new estimates of surface temperature and emissivities. The training of the NN is carried out on an independent training dataset composed of radiative transfer

(RT) simulations performed with the RTTOV model. The emissivities are the TELSEM outputs and the emissivity FGs are the same emissivities perturbed by a FG error noise equal to the TELSEM errors.

After the training stage, the NN inversion scheme can be tested on real AQUA measurements. The FG information is provided by the TELSEM estimates and the ECMWF analysis gives the surface skin temperature. The NN estimates new values for both variables. In order to test their quality, RT simulations are performed using, similarly to section 3.1, the ECMWF analysis plus surface information. Figure 6 presents the RMS differences between the RT simulations and the real observations (calibrated) when the FG or retrieved surface information are used. Four configurations are tested: (1) surface comes from the FG, (2) only emissivities come from the NN retrieval, (3) only the skin temperature comes from the NN retrieval and (4) both emissivities and surface skin temperature come from the NN retrieval. These statistics allow us to measure the impact of improving emissivity and temperature on the retrieval scheme. It should be noted here that since the retrieval uses a NN method, it uses a general inversion model not specific to each situation to be inverted. By contrast, a 1D-Var retrieval scheme should be even more efficient in bringing together RT simulations and real satellite observations because the inversion process, in this case, is dedicated to each new observation.

The results are very encouraging. Both retrieved skin temperature and emissivities have a significant impact on bringing RT simulations and calibrated observations closer. This shows that even if TELSEM estimates are good, they can be improved by a retrieval scheme by more than 1 K for some horizontally polarized channels. It is well known that the skin temperature from operational analysis is not accurate enough, and the impact of using a retrieved surface temperature,  $T_s$ , instead of the analysis is even greater than for the emissivities: almost 1.5 K for both horizontally and vertically polarized channels. Of course, no impact was found for the water-vapour sounding channels at 183 GHz. It is also very interesting to note that when both retrieved  $T_s$ s and emissivities are used, the impact is even better and larger than just the sum of the contribution

of both. This means that there is synergy in retrieving, together,  $T_s$  and emissivities (Aires *et al.*, 2001, 2011; Aires, 2011). This experiment shows clearly that the TELSEM emissivities are a good FG that can be improved by a retrieval scheme, and that this retrieval benefits from the simultaneous retrieval of both surface skin temperature and emissivities.

#### 4. Conclusion

A Tool to Estimate Land-Surface Emissivities at Microwave frequencies (TELSEM) has been developed within the RTTOV radiative-transfer model, for a simple and convenient use by a large community. This new facility allows us easily to build surface microwave-emissivity climatologies that can be used as a realistic FG in emissivity-estimation schemes and/or atmospheric retrieval algorithms over land, including variational assimilation.

TELSEM is anchored to a reference-emissivity climatology calculated from SSM/I observations. It is able to interpolate in frequencies and viewing angles for both linear polarizations. It is originally designed for frequencies between 19 and 85 GHz, but tests proved that it is beneficial down to 6 GHz and up to 190 GHz. TELSEM also provides the full covariance matrix of the uncertainties in the interpolated emissivities, key information for most retrieval algorithms, especially for assimilation in NWP schemes.

The potential benefits of TELSEM for the inversion of surface-sensitive microwave sounding channels are illustrated by three examples. First, the emissivity interpolator has been used within the RTTOV model to simulate NOAA-17 AMSU-A and -B instruments and compare the results with the corresponding real observations. Adding the land-surface emissivity information from TELSEM has a strong positive impact, with a decrease of the RMS statistics of more than 10 K for some channels, averaged over two months on a continental scale. Using these realistic land-surface emissivity FG estimates, the agreement between simulations and observations is similar over land and ocean, making it possible to attempt assimilation of surface-sensitive observations over the continents. A water-vapour atmospheric retrieval experiment has been conducted, from combined AMSR-E and HSB data, using an adaptation of the operational chain developed for the future Megha-Tropiques mission. The ability to reproduce the observed TBs over land directly benefits the retrieval of the lower atmospheric layer, with retrieval accuracy comparable over land and ocean. Furthermore, it has been shown that the TELSEM emissivity FGs can be significantly improved when they are updated by a simple statistical retrieval scheme. TELSEM in RTTOV will be soon tested in an assimilation scheme in a NWP centre.

This study was supported by the NWP-Satellite Application Facility. A similar effort is being conducted toward the development of an infrared land-surface emissivity calculator, based on previous work by Seemann *et al.* (2008). Using these two emissivity tools with RTTOV will allow microwave and infrared measurements to be assimilated in retrieval schemes over land benefiting from their synergy (Aires, 2011; Aires *et al.*, 2011).

#### Acknowledgement

This work has been performed in the framework of the Visiting Scientist Programme of the EUMETSAT Satellite Application Facility on Numerical Weather Prediction (NWP SAF), <http://www.nwpsaf.org>

#### References

- Aires F. 2011. Measure and exploitation of multi-sensor and multi-wavelength synergy for remote sensing Part I – Theoretical considerations. *J. Geophys. Res.* 116: D02301, DOI: 10.1029/2010JD014701.
- Aires F, Bernardo P, Brogniez H, Prigent C. 2010. An innovative calibration method for the inversion of satellite observations. *J. Appl. Meteorol.* 49(12): 2458–2473.
- Aires F, Paul M, Prigent C, Rommen B, Bouvet M. 2011. Measure and exploitation of multi-sensor and multi-wavelength synergy for remote sensing: Part II – Application for the retrieval of atmospheric temperature and water vapour from METOP. *J. Geophys. Res.* 116: D02303, DOI: 10.1029/2010JD014702.
- Aires F, Prigent C, Rossow WB, Rothstein M. 2001. A new neural network approach including first guess for retrieval of atmospheric water vapour, cloud liquid water path, surface temperature and emissivities over land from satellite microwave observations. *J. Geophys. Res.* 106: D14887–14907.
- Aires F, Prigent C, Rossow WB. 2005. Sensitivity of microwave and infrared satellite observations to soil moisture at a global scale. II: Global statistical relationships. *J. Geophys. Res.* 110: D11103, DOI: 10.1029/2004JD005094.
- Deblonde G, English SJ. 2001. ‘Evaluation of the FASTEM-2 fast microwave oceanic surface emissivity model’. In *Tech. Proc. ITSC-XI Budapest*, 20–26 Sept 2000; pp. 67–78. ITWG/IAMAS: Budapest.
- Desbois M, Capderou M, Eymard L, Roca R, Vilard N, Violier M, Karouche N. 2007. Megha-Tropiques: un satellite hydro météorologique franco-indien. *La Météorologie* 57: 19–27.
- English SJ, Hewison T. 1998. A fast generic millimetre wave emissivity model. *Microwave remote sensing of the atmosphere and environment*. Proc. SPIE 3503: 22–30.
- Eyr JR, Woolf HM. 1988. Transmittance of atmospheric gases in the microwave region: a fast model. *Appl. Opt.* 27: 3244–3249.
- Jimenez C, Prigent C, Aires F. 2009. Toward an estimation of global land surface heat fluxes from multisatellite observations. *J. Geophys. Res.* 114: D06305, DOI: 10.1029/2008JD011392.
- Karbou F, Aires F, Prigent C, Eymard L. 2005a. Potential of AMSU-A and -B measurements for atmospheric temperature and humidity profiling over land. *J. Geophys. Res.* 110: D07109, DOI: 10.1029/2004JD005318.
- Karbou F, Prigent C, Eymard L, Pardo J. 2005b. Microwave land emissivity calculations using AMSU measurements. *IEEE Trans. Geosci. Remote Sensing* 43: 948–959.
- Matricardi M, Chevallier F, Kelly GA, Thépaut J-N. 2004. An improved general fast radiative-transfer model for the assimilation of radiance observations. *Q. J. R. Meteorol. Soc.* 130: 153–173.
- Pellerin T, Wigneron J-P, Calvet J-C, Waldeleuf P. 2003. Global soil moisture retrieval from a synthetic L-band brightness temperature data set. *J. Geophys. Res.* 108: 4364, DOI: 10.1029/2002JD003086.
- Prigent C, Rossow WB, Matthews E. 1997. Microwave land-surface emissivities estimated from SSM/I observations. *J. Geophys. Res.* 102: 21867–21890.
- Prigent C, Aires F, Rossow WB, Matthews E. 2001. Joint characterization of vegetation by satellite observations from visible to microwave wavelength: A sensitivity analysis. *J. Geophys. Res.* 106: 20665–20685.
- Prigent C, Chevallier F, Karbou F, Bauer P, Kelly G. 2005a. AMSU-A land-surface emissivity estimation for numerical weather prediction assimilation schemes. *J. Appl. Meteorol.* 44: 416–426.
- Prigent C, Munier J, Thomas B, Ruffié G. 2005b. Microwave signatures over carbonaceous sedimentary platforms in arid areas: Potential geological applications of passive microwave observations? *Geophys. Res. Lett.* 32: L23405, DOI: 10.1029/2005GL024691.
- Prigent C, Aires F, Rossow WB. 2006. Land surface microwave emissivities over the globe for a decade. *Bull. Am. Meteorol. Soc.* 87: 1573–1584, DOI: 10.1175/BAMS-87-11-1573.
- Prigent C, Papa F, Aires F, Rossow WB, Matthews E. 2007. Global inundation dynamics inferred from multiple satellite observations, 1993–2000. *J. Geophys. Res.* 112: D12107, DOI: 10.1029/2006JD007847.
- Prigent C, Jaumouille E, Chevallier F, Aires F. 2008. A parametrization of the microwave land-surface emissivity between 19 and 100 GHz,

- anchored to satellite-derived estimates. *IEEE Trans. Geosci. Remote Sensing* **46**: 344–352.
- Rossow WB, Schiffer RA. 1999. Advances in understanding clouds from ISCCP. *Bull. Am. Meteorol. Soc.* **80**: 2261–2288. DOI:10.1175/1520-0477.
- Saunders R, Matricardi M, Brunel P. 1999. An improved fast radiative-transfer model for assimilation of satellite radiance observations. *Q. J. R. Meteorol. Soc.* **125**: 1407–1425.
- Seemann SW, Borbas EE, Knuteson RO, Stephenson GR, Huang H-L. 2008. Development of a global infrared land-surface emissivity database for application to clear sky sounding retrievals from multispectral satellite radiance measurements. *J. Appl. Meteorol. Clim.* **47**: 108–123.
- Weng F, Yan B, Grody NC. 2001. A microwave land emissivity model. *J. Geophys. Res.* **106**: 20115–20123.
- Weng F, Han Y, van Delst P, Liu Q, Kleespies T, Yan B, Le Marshall J. 2005. JCSDA Community Radiative Transfer Model (CRTM). In *International TOVS Study Conference, 14th, Beijing, China, 25–31 May 2005 (proceedings)*, pp. 217–222. University of Wisconsin-Madison, Space Science and Engineering Center, Cooperative Institute for Meteorological Satellite Studies (CIMSS): Madison, WI.